AGU100 ADVANCING EARTH AND SPACE SCIENCE

Water Resources Research

RESEARCH ARTICLE
10.1029/2017WR021819

# Combining Experimental Methods and Modeling to Quantify the Complex Recharge Behavior of Karst Aquifers

**M. Mudarra[1], A. Hartmann[2,3], and B. Andreo[1]**

[1]Department of Geology and Centre of Hydrogeology at the University of Malaga (CEHIUMA), University of Malaga, Malaga, Spain, [2]Institute for Hydrology, Freiburg University, Freiburg, Germany, [3]Department of Civil Engineering, University of Bristol, Bristol, UK

**Key Points:**
- The lumped VarKarst model is used to assess allogenic and autogenic contributions to the recharge of karst systems
- Coupling field data by a new estimation parameter procedure serves to confine ambiguity of the water budget estimated with two other methods
- Mutual evaluation between conceptual and numerical modeling approaches must be constantly conducted to enhance knowledge of karst systems

**Supporting Information:**
- Data Set S1
- Data Set S2

**Correspondence to:**
M. Mudarra,
mmudarra@uma.es

**Citation:**
Mudarra, M., Hartmann, A., & Andreo, B. (2019). Combining experimental methods and modeling to quantify the complex recharge behavior of karst aquifers. *Water Resources Research*, *55*, 1384–1404. https://doi.org/10.1029/2017WR021819

Received 25 SEP 2017
Accepted 13 JAN 2019
Accepted article online 17 JAN 2019
Published online 20 FEB 2019



**Abstract** Integration of the abundant information derived from different sources, characterizing techniques and modeling methodologies, is crucial for extending our knowledge of karst aquifers and their available water resources. In this work, a numerically based approach derived from an improved version of the lumped VarKarst model is proposed, which jointly considers spring discharge and dye test results in calibration routine, to assess independently the contribution of the allogenic and autogenic components to the total recharge of a complex karst system with proved duality in its recharge mechanisms. A newly developed parameter estimation procedure based on rather soft performance rules is employed to confine the uncertainty of the water budget previously obtained with two other independent methods (Soil Water Balance and APLIS). Unlike other methodologies that lead to semiquantitative estimations of input sources, results from our approach display reliable ranges of calibrated values for recharge rate, recharge area, and, to a lesser extent, for water runoff infiltration coming from the streamflow. The integration of all these quantitative results with data (qualitative) previously derived from other experimental methodologies has meant a significant advance in understanding the behavior of the pilot system, allowing a more realistic and robust conceptual model to be developed. We conclude by emphasizing that a continuous transfer of improvements from conceptual to numerical modeling approaches, and vice versa, is necessary to enhance knowledge of carbonate aquifer functioning and ultimately achieve better evaluation and management of water resources. During this process, frequent mutual evaluation between the modeling approaches must be performed.

## 1. Introduction

Advances in the knowledge of carbonate aquifers have been accompanied by the simultaneous development of modeling approaches, both conceptual (schematic understanding of the hydrogeological system) and particularly mathematical procedures (Hartmann, Goldscheider, et al., 2014; Kiraly, 1998; Kovacs & Sauter, 2007). In the latter category, there is an increasing number of numerical models (distributed, lumped, and hybrid) performed for simulating karst aquifers with a broad range of purposes: from the integrated hydrodynamic analysis (Kovacs & Sauter, 2007; Mazzilli et al., 2017) to the simulation of karst hydrology and the prediction of water resources under the impact of the global climate change (Hartmann et al., 2015; Rodríguez et al., 2013; Scanlon et al., 2003). Nevertheless, the hydrogeological heterogeneity and the high complexity of karst media resist simplifications when flow and transport processes are numerically simulated. In many cases, difficulties in collecting sufficient information about karst system properties (spatial and temporal) or limited data from observation points (springs, boreholes, caves, etc.) lead to uncertainty in the conceptualization and parameterization and hence in the processes representation and application of model approaches (Jukic & Denić-Jukić, 2009; Le Moine et al., 2008). The lack of available data imposes constraints particularly on spatially distributed models, which required higher resolution of input data (e.g., groundwater potential distribution and spatial distribution of the karstified horizons) for acceptable simulation and prediction results (Oehlmann et al., 2013; Saller et al., 2013). In contrast, lumped models have shown adaptability and strength in simulating the hydrogeological behavior under different contexts and scales (Hartmann et al., 2015), since data requirements for model inputs are less rigorous. However, parameterization in this last type of approaches cannot be determined directly from physical measureable processes.

To attain greater realism in simulations, adapted lumped models have progressively included in their structure more parameters, trying to capture some distinctive properties of karst aquifers at different scales: individual conduit and matrix flows (Fleury et al., 2009; Schmidt et al., 2014), recharge and storage in the soil and epikarst (Hartmann et al., 2012; Tritz et al., 2011), discharge by various springs (Rimmer & Salingar, 2006), and distinction between internal and external runoff (Bailly-Comte et al., 2012; Jukic & Denić-Jukić, 2009; Le Moine et al., 2008), among others. In these examples, the values of the model parameters are typically determined by calibrating the hydrodynamic responses of aquifers, with hydrologic models that use mathematical expressions based on linear or nonlinear relations between the system's flow and its storage dynamics. Approaches that have incorporated other hydrological variables in calibration routine, such as hydrochemistry and water isotopes, are less common due to their limitations in reflecting the physical processes of the whole karst system. Some authors have incorporated additional field data such as hydrochemical information (Charlier et al., 2012; Hartmann et al., 2013, 2016; Pinault et al., 2001) or gravimetric information (Mazzilli et al., 2013) to the calibration and evaluation tasks, reaching higher predictive capacities than if discharge data were exclusively used in the model. With the same aim, information from different data sources have been successfully used for calibration in both distributed and lumped modeling approaches performed in karst systems as well as in other hydrogeological environments (e.g., Ghasemizadeh et al., 2012; Schwerdtfeger et al., 2016). It could be expected, consequently, that integrating further types of independent field observations, such as tracer test results, would help reduce the inherent ambiguity found in lumped-based modeling procedures, reinforcing its skills in the simulation and evaluation of karst water resources and in the analysis of the hydrological processes involved.

Tracing techniques are one of the most effective tools to unambiguously confirm subsurface hydraulic connections and transport dynamics (i.e., along a flow path), to delineate allogenic and autochthonous catchment areas of karst springs and, in general, to better understand surface water-groundwater relationships (Benischke et al., 2007; Goldscheider et al., 2008; Käss, 1998). Most modeling research including dye tracing data is focused on the quantitative assessment of transport properties in karst systems (e.g., Field & Pinsky, 2000; Maloszewski et al., 1998) and estimation of the relevant reactive transport parameters and conduit geometry (Birk et al., 2005; Geyer et al., 2007; Luhmann et al., 2012). Tracing techniques may also apply spatially lumped hydrologic models to conceptualize the transport of the artificial tracer through the karst system, considering convection, dispersion, mixing, separate flow paths through different conduits, and exchange of the tracer with the matrix (Maloszewski, 1994; Maloszewski et al., 1998). However, no research effort to date addresses prognostic simulations of water resources at the whole catchment scale of carbonate aquifers, by integrating dye tests data in the lumped modeling structure. Only Oehlmann et al. (2015) partially attempted this approach, combining specific hydraulic data, spring discharge, and several tracer breakthrough curves (BTCs) in a hybrid model for simulating groundwater flow and transport in a heterogeneous karst aquifer with a well-defined catchment area of 150 $km^2$. Therefore, there is clearly room for improvement in karst water resources evaluation and projection, and the inclusion of additional information derived from tracer tests can strengthen the parameter calibration procedure.

Because of their inherent simplifications, numerical approaches always entail some uncertainty and their results are insufficient for drawing reliable quantitative conclusions. They should always be compared with results derived from other independent experimental methodologies applied in karst hydrogeology, which have been used, jointly with the compression of the geological and hydrogeological frameworks, to establish conceptual models of carbonate aquifers (Bakalowicz, 2005; Drogue, 1980; Ford & Williams, 2007; Goldscheider & Drew, 2007; Mangin, 1975). Integrating experimental methods (to derive conceptual models) and simulation approaches rather than applying them independently is a persistent challenge in hydrological sciences (Seibert & McDonnell, 2002).

n this study, a modified version of the lumped VarKarst model (Hartmann et al., 2013) was performed to quantitatively assess the contribution of allogenic and autogenic components to the total recharge of a small and mountainous karst system, with imprecisions in the extent of its catchment area but proved duality in recharge mechanisms (binary karst system). To do this, the novel calibration routine takes jointly into consideration discharge and dye tracer concentrations. A new parameter estimation procedure based on Kling-Gupta efficiency (*KGE*; Gupta et al., 2009) was employed to reduce and quantify the intrinsic uncertainty found during the simulations of the water budget components. The prior ranges of the model parameters

were confined considering the information derived from two other independent methods for water resources evaluation (Soil Water Balance [SWB] using Thornthwaite equation—1948—and APLIS approach—Andreo et al., 2008; Marín, 2009) and also from field investigation. The simultaneous application of different methodologies provided a reliable assessment of some significant water budget components (runoff infiltration, recharge area, and recharge rates) and, ultimately, of the water resources availability, whereas other methods based exclusively on hydrochemical observations (coefficient of variations, CV%, of electrical conductivity, EC; Worthington et al., 1992) lead to semiquantitative estimations of the input sources. From these results, an improved conceptual model of the system and its behavior was established, more solid than if experimental or modeling approaches had been employed individually. Hence, such coupling of knowledge from experimental and modeling approaches might open new perspectives that enhance characterization of carbonate (karst) aquifers and lead to a better evaluation and management of water resources.

## 2. Experimental Area and Background Information

The pilot site to test the methodological approach proposed in present work is the Auta karst system, located approximately 30 km NE of the city of Malaga in Southern Spain (Figure 1a). It is an aquifer or hydrogeological system whose catchment area is not well defined yet within a larger mountainous area known as the Sierra de Enmedio and Los Tajos area. The terrain in this zone is rough, sometimes very steep, with altitudes ranging from 600 to 1,415 m above sea level (ASL) and including almost-vertical rock faces rising over 100 m named Los Tajos (1,250 m ASL). The climate is temperate Mediterranean, with a marked seasonal pattern in the annual variations of precipitation and air temperature. Rainfall occurs mainly from autumn to spring time, associated with wet winds coming from the Atlantic Ocean. Climate conditions are also characterized by a dry season (very often of up to 3–4 months), practically without rain, in summer. The mean annual precipitation recorded in this area during the period 1968/1969 to 2009/2010 was around 825 mm, with a spatial distribution influenced by the altitude: it was below 775 mm in the lower parts (southern border) and up to 900 mm in the higher areas (Mudarra, 2012). The research time period involved in the present work (October 2006 to September 2009) could be considered slightly dry, with an average precipitation of 713 mm, calculated from isohyets maps. The air temperature records for the north (over 925 m ASL) and south (over 550 m ASL) edges of the system show mean annual values of 13 and 17 °C, respectively (Mudarra, 2012).

Geologically, the experimental site and the other reliefs that make up the Sierra de Enmedio and Los Tajos area are situated within the Betic Cordillera; it consists of 450- to 500-m thick Jurassic dolostones and limestones (Figure 1a), which present Upper Triassic clays, dolomitic beds, sandstones and evaporite rocks (mainly gypsum) at the bottom, and Lower Cretaceous-Tertiary marly limestones, marls, and silexites at the top (Martín-Algarra, 1987; Peyre, 1974). The geological structure is complex, defined by the overlapping of two tectonic units (Los Tajos unit and Sierra de Enmedio unit) with general vergence toward the SW (Figure 1). Los Tajos unit occupies the lowest tectonic position, and it is characterized by the existence of an NNE-SSW anticlinorium dome in whose core some inverse faults developed with vergence toward the south, affecting clayey and marly materials (Figure 1b). In turn, the Sierra de Enmedio consists of a NW-SE anticline fold, whose SW flank overthrusts the Los Tajos unit. Between the two units and surrounding them appear outcrops of Flysch-type clays and sandstones. The entire structure is affected by more recent strike-slip faults (NW-SE) and normal fractures (NE-SW and N-S) which configure the geological structure and orography of the area. The predominance of Jurassic oolitic limestones outcrops, densely fractured, reinforced karstification and a noteworthy development of exokarst landforms, especially at higher altitudes and over Los Tajos carbonate outcrops (Mudarra, 2012). In these areas, large karrenfields exist over bare carbonate rocks. A patchy soil cover up to 10–15 cm thick can be found, especially where slope is low. Overall vegetation is scarce, with mainly Mediterranean shrub growth on the patchy soils.

In hydrogeological terms, the Sierra de Enmedio and Los Tajos aquifer is formed by fractured and karstified Jurassic carbonate rocks (21 $km^2$), limited by low-permeability materials at all their borders (Flysch clays, Cretaceous-Tertiary marls, and Tertiary silexites). The geometry is particularly determined by the anticlinal core of the Sierra de Enmedio (Triassic clays) and occasionally by NW-SE strike-slip faults that individualize several hydrogeological sectors in Los Tajos area (Figure 1a). In contrast, carbonate rocks outcropping at the southwestern flank of Sierra de Enmedio and Los Tajos area are connected below the exposed Flysch clays (NW-SE inverse fault), where an open limit between the banks of the Sabar River is defined.

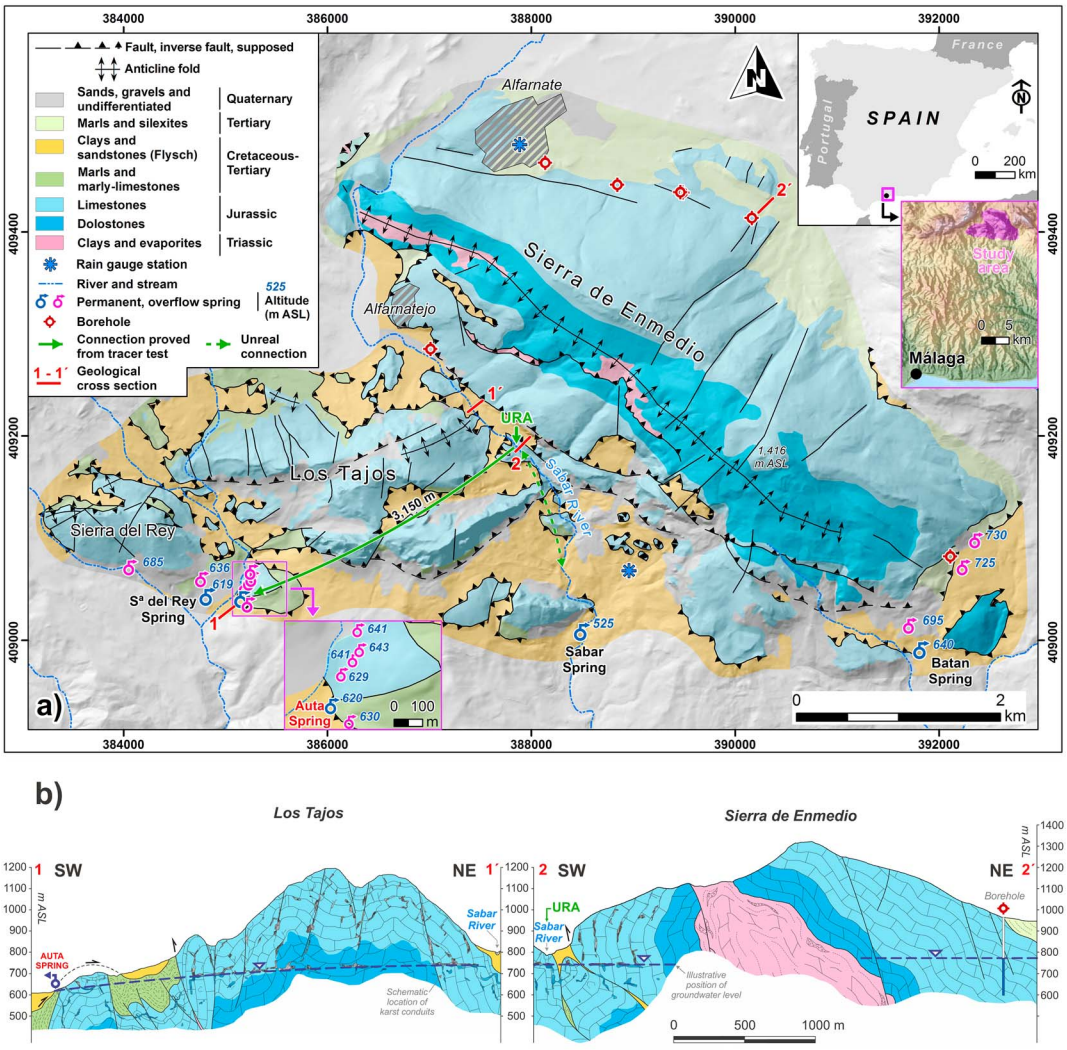


**Figure 1.** Geological-hydrogeological sketch (a) and cross sections (b) of the Sierra de Enmedio and Los Tajos area and its location in Southern Spain. Elevation in meters above sea level (m ASL).

Accordingly, lateral inflow from the southwestern flank of Sierra de Enmedio toward Los Tajos area may occur, with consequent changes in the apparent catchment area of the autogenic component of the Auta system, from 3.4 $km^2$ (considering exclusively Los Tajos carbonate outcrops) to 8.8 $km^2$ (including the SW flank of Sierra de Enmedio). The supposed hydrogeological connections imply the existence of a continuous groundwater potential level, whose spatial distribution is difficult to determine given the absence of observation points. Despite this lack of information, an illustrative approximation of the vertical position of the groundwater level is included in Figure 1b, to reflect intermediate water conditions within the system.

Groundwater discharge occurs mainly in a natural regime through a considerable number of springs along the southern border of the carbonate outcrops. The most significant is the Auta permanent spring, at 620 m ASL, on the southwestern edge of Los Tajos area (Figure 1). During high water conditions up to five overflow springs appear gradually in this sector, from 629 to 643 m ASL. The annual mean discharge rate from Auta spring during the study period was 90 L/s. This value includes sporadic contributions from overflow springs. Other significant and permanent outlet points have been found in the Sierra de Enmedio and Los Tajos area, from 525 to 640 m ASL. Previous studies highlighted the considerable hydrogeological complexity of the zone, related to the geological-structural framework and to the relative role that unsaturated and saturated zones play in the hydrogeological functioning of each sector of the aquifer (Mudarra, 2012; Mudarra et al.,

2012). In the case of the Auta system, a certain independence in the behavior of both zones was inferred through analysis of the hydrothermal and hydrochemical responses of the permanent (Auta) and nonpermanent (overflow) springs during recharge periods. Due to the absence of boreholes, no quantitative data on the hydraulic properties of the pilot site are available. There are no inventoried caves or speleological developments known in this area, yet a certain degree of functional karstification in the unsaturated zone of the Auta system must exist, inferred indirectly after monitoring the hydrogeological responses of the overflow springs (Mudarra et al., 2012) and as Figure 1b schematically shows.

The Auta karst system constitutes the sole source of drinking water for a nearby urbanized area having 3,000 inhabitants. Hydrogeochemical tools applied to this site revealed the existence of an incipient degree of contamination affecting the system on a whole (Mudarra et al., 2011, 2012), whose origin could be associated with the infiltration of surface runoff water through the Sabar riverbed. This stream receives partially treated waste water from two villages (1,600 inhabitants) placed at the Sabar head basin (Alfarnate and Alfarnatejo in Figure 1a).

## 3. Materials and Methods

### 3.1. Workflow and Data Sources

Because model structures should be supported by a solid knowledge of the system, all geological and hydrogeological information about the pilot site was reviewed before applying the numerical modeling approach. The available information led to the development of a preliminary conceptual model for the Auta system, establishing the hydrogeological characteristics and functioning of this site (Mudarra et al., 2012). In the framework of this study, the corpus of background knowledge was updated after applying tracing techniques and water balance calculations, the latter by means of the SWB and the APLIS methods.

Coupled numerical simulations of the hydrodynamic behavior of the karst system and the tracer BTC recorded at Auta spring were performed using a modified version of the lumped VarKarst model (Hartmann et al., 2013). Together with the use of a new parameter estimation approach, this made it possible to evaluate the contribution of the allogenic and autogenic (including the catchment area) components of the water budget to the total recharge of the system. Finally, all information was integrated to create a new and improved conceptual model for the pilot site. Detailed descriptions about the different methodological procedures employed in this work are offered in the following sections, whereas Figure 2 schematizes the overall workflow.

The geomorphological (karst landforms) and hydrogeological (EC, water temperature, discharge, and dye test data) information used in this study were obtained for research purposes by the staff of the Centre of Hydrogeology of the University of Malaga. In situ EC and water temperature values were taken using a conductivity/temperature meter (WTW™ conductivimeter-thermometer 340i), whereas spring discharge data from single measurements using the area-velocity method (OTT™ C2 flowmeter). Meteorological and lithological information were, respectively, provided by the databases of the Spanish Agency of Meteorology (AEMET) and the Spanish Geological Survey (IGME). Finally, digital elevation data and the spatial distribution of the types of soil were supplied by the Spanish National Geographical Institute (IGN). Availability and properties of the different databases used in this research are described in Table 1.

### 3.2. Dye Tracing

To check the hydrogeological connection between Sabar River and the springs draining the Sierra de Enmedio and Los Tajos area, 500 g of uranine (Fluorescein Sodium, CAS: 518-47-8) was poured into the streamflow, at a point located at 795 m ASL (Figure 1a) and where infiltration of runoff water (3–4 L/s) through the carbonate riverbed and alluvial deposits was initially perceived. From this point, a sinking streambed of 400-m length was identified downstream, being its lowest stretch located at 715 m ASL. Tracer injection occurred at 10:30 p.m. on 27 June 2011, under low-flow hydrological conditions. In other scenarios (high or intermediate water conditions), a great fraction of dye mass dissolved in runoff water would be displaced downstream (no sinkhole exists). Sabar River is exclusively fed by runoff water generated at its head-catchment area during rainfall periods. In fact, river streamflow became definitively dry 4 days after injection, although some water could flow within the alluvial deposits afterward.

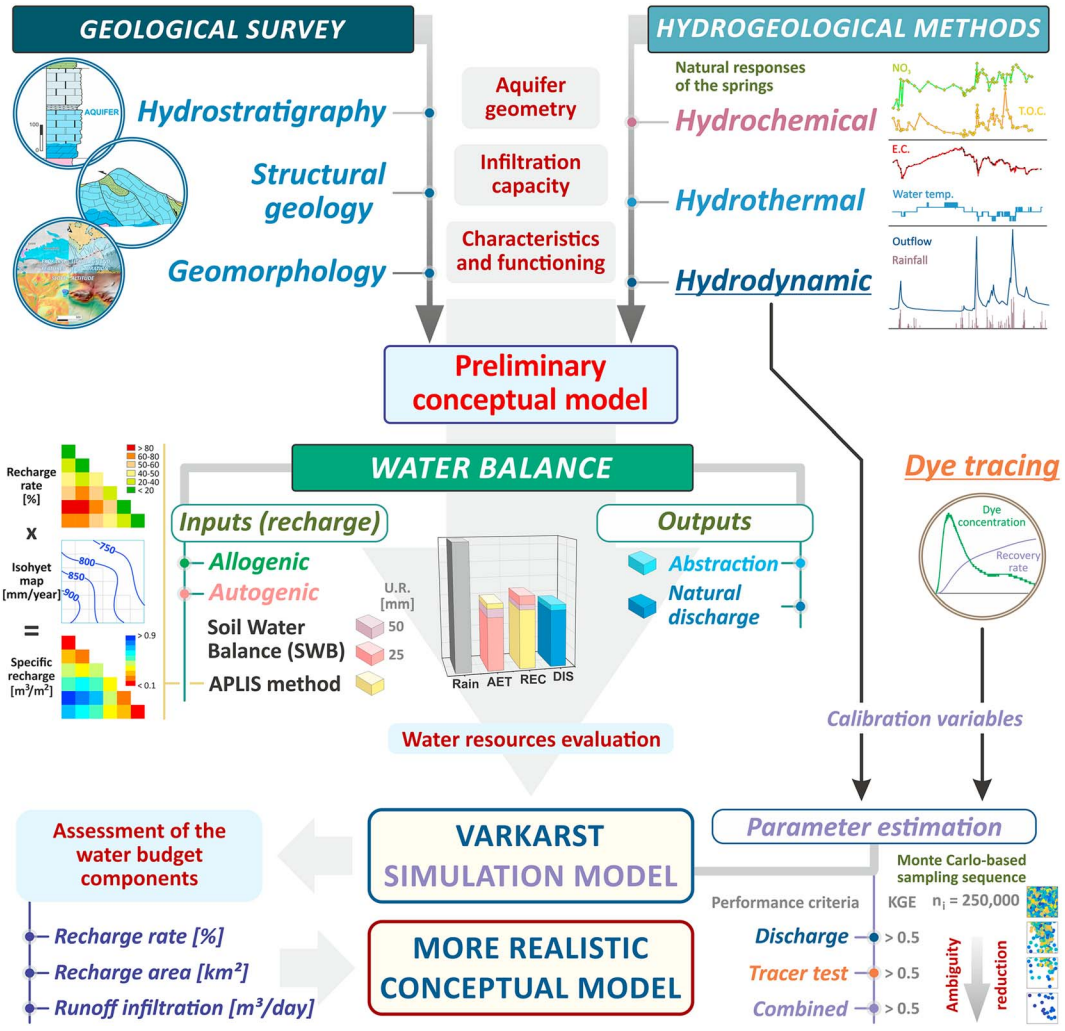


**Figure 2.** Schematic representation of the workflow addressed in this research, including the parameter estimation routine of VarKarst model.

Sampling at all permanent outflow points started 2 hr before injection (to detect unequivocally the arrival of the tracer) and finished 1 month later (27 July; Table 1). During this time, 45 water samples (eight from Auta spring) were manually collected in 60-ml dark glass bottles (transported and stored in darkness), with increasing periodicity from 3 to 7 days, for subsequent dye determination in the laboratory of the Centre of Hydrogeology of University of Malaga (Perkin-Elmer® LS55 spectrofluorometer, synchronous scan procedure). The analytical detection limit for dye was 0.04 μg/L. Sample analyses were performed within 24 hr. To complement ordinary sampling procedures, a GGUN-FL30 flow-through field fluorometer was installed in Auta spring during the same time period. This device continuously records (measurement each 15 min) the dye concentrations in the outflow water.

### 3.3. Water Balance Estimation

To assess the water budget of the Sierra de Enmedio and Los Tajos area, where the Auta system is included, total discharge (spring outflows and pumping abstractions) and autogenic components of recharge (diffuse infiltration) were evaluated for the study period. In all cases, mean annual discharge of the springs (Figure 1a) was calculated through the mathematical integration of hydrographs (plotted from single measurements; Table 1). Likewise, two independent methods for diffuse recharge estimation were applied (Table 1): SWB using the Thornthwaite approach (1948) and APLIS method (Andreo et al., 2008; Marín, 2009).

**Table 1**
*Data Availability and Data Properties of the Variables Used by the Methods Applied in This Research*

| Method | Variable | Unit | Spatial resolution | Time period | Frequency | Source |
|---|---|---|---|---|---|---|
| Dye tracing | | | | | | |
| | Dye concentration | µg/L | Individual locations | 27 June to 27 July | 15 min | CEHIUMA |
| | Mass recovery | g (%) | Individual locations | Individual period | — | CEHIUMA |
| Water budget | | | | | | |
| Discharge | Natural discharge | L/s; $hm^3$/year | Individual locations | October 2006/September 2009 | Daily–weekly | CEHIUMA |
| | Abstractions | $hm^3$/year | Individual locations | October 2006/September 2009 | Weekly–monthly | CEHIUMA |
| Autogenic recharge | Carbonate rock areas | $km^2$ | Vector data | — | — | IGME |
| Soil Water Balance | Precipitation | mm/day | Individual locations | October 2006/September 2009 | Daily | AEMET |
| (SWB) | Air temperature | °C | Individual locations | October 2006/September 2009 | Daily | AEMET |
| APLIS | Digital Elevation Model | m ASL | raster 5 × 5-m cell size | — | — | IGN |
| | Lithology map | — | Vector data | — | — | IGME |
| | Karst landforms | — | Vector data | — | — | CEHIUMA |
| | Soil type map | — | Vector data | — | — | IGN |
| | Precipitation | mm/year | Vector data | October 2006/September 2009 | Annual | CEHIUMA |
| VarKarst model | | | | | | |
| | Spring discharge | L/s | Individual locations | October 2006/September 2009 | Daily | CEHIUMA |
| | Dye concentration | µg/L | Individual locations | 27 June to 27 July | Daily | CEHIUMA |

*Note*. Source: Center of Hydrogeology of the University of Málaga (CEHIUMA), Spanish Geological Survey (IGME), Spanish Agency of Meteorology (AEMET), Spanish National Geographical Institute (IGN).

Evaluation of the recharge volume by the SWB considers daily precipitation ($P$) and mean daily air temperature data ($T$), obtained from local meteorological stations, to calculate the actual evapotranspiration (AET) and, therefore, the effective precipitation ($P$ - AET). Given the edaphic characteristics of the study area, two different values of useful reserve ($UR$) in the soil, 25 and 50 mm, were applied as input in the approach. The hydraulic characteristics of the patchy soil covering the carbonate bedrocks were defined according to the predominant thickness (10- to 15-cm maximum) and texture (silty clayey) of the edaphic layer (leptosol type), after in situ observations. The resulting values were multiplied by the surface of carbonate outcrops, considering that all runoff over that area becomes aquifer recharge due to karst features. Calculations were made using the software TRASERO v2.0 (Padilla & Delgado, 2013) and spatial analysis tools from Geographic Information System (GIS) afterward.

The APLIS method (Andreo et al., 2008) is a GIS-based approach that was developed to estimate the mean annual recharge (autogenic) that take places in carbonate aquifers, expressed as a percentage of precipitation (recharge rate). Input parameters are average annual precipitation, its spatial distribution, and a combination of the physical variables found to be the most influential: altitude ($A$), slope ($P$), lithology ($L$), infiltration landforms ($I$), and soil type ($S$). To obtain a map of the average recharge rates, previous information is transformed following rating criteria and subsequently corrected by a factor ($F_{hj}$, ranging between 0.1 and 1), depending on the permeability of the exposed lithologies (Marín, 2009)

$$\overline{R}_j = \frac{A_j + P_j + 3L_j + 2I_j + S_j}{0.9} \cdot F_{h.j} \quad (1)$$

Multiplying annual rainfall (spatially distributed) by the infiltration coefficient map (equation (1); Figure 2) and by the surface of carbonate outcrops, also using spatial analysis tools from GIS, the mean annual recharge during the study period was calculated. Additional detailed information about the methodological procedure of this method was described in previous works (Andreo et al., 2008; Hartmann, Mudarra, et al., 2014; Marín, 2009). The APLIS approach has been successfully applied to other carbonate aquifers worldwide representative of a varied range of climatic and geological contexts (Gerner et al., 2012; Hartmann et al., 2016; Zagana et al., 2011).

### 3.4. Numerical Modeling

To estimate the recharge components of Auta system (runoff infiltration, recharge rates, and recharge area), the simulation model VarKarst (Hartmann et al., 2013) was applied to jointly simulate records of spring discharge and dye tracer concentrations (Table 1 and Figure 2). A newly developed parameter estimation

procedure is used to confine the ambiguity of the water budget and to provide quantitative information on its components, as well as to quantify the remaining uncertainty in their calculations.

#### 3.4.1. The Model Approach

VarKarst model considers the variability of karst system properties by means of statistical distribution functions. Similar to the Probability Distributed Model (Moore, 2007) or the variable karst recharge model (Hartmann et al., 2012), VarKarst includes the spatial variability of (i) soil and epikarst depths, (ii) fractions of concentrated and diffuse recharge to the groundwater, (iii) epikarst hydrodynamics, and (iv) groundwater hydrodynamics by Pareto functions that are applied to a set of $N$ model compartments (15 in the current version of VarKarst). Hence, a range of variably dynamic pathways is simulated through the karst system. The detailed equations of the model hydrodynamics are described in the Appendix A and also by Hartmann et al. (2013), Hartmann, Mudarra, et al. (2014), and Hartmann et al. (2016). Runoff infiltration (allogenic recharge) was not considered in previous versions of the model. In the current case, daily river infiltration $Q_{\mathrm{inf}}(t)$ (mm) is included by defining a maximum discharge rate of the river $Q_{\mathrm{river,max}}$ (L/s) that determines the volume entering the karst system

$$Q_{\mathrm{inf}}(t) = \frac{\min\left[Q_{\mathrm{river,\,max}}, Q_{\mathrm{river}}(t)\right] \cdot 86,400 \ \mathrm{s}}{A} \tag{2}$$

where $Q_{\mathrm{river}}(t)$ is the streamflow of the river (L/s), which is rescaled by the number of seconds of 1 day (86,400 s), and $A$ is the recharge area of Auta spring (km$^2$). Input range of $Q_{\mathrm{river,max}}$ is defined following previous in situ observations in the field and considering the results from the general water budget assessment (Figure 2). $Q_{\mathrm{inf}}(t)$ is added to percolating water from the soil entering the epikarst (see Appendix A). The attribution of large parts allogenic recharge $(N-1)/N$ to the model flow paths that represent diffuse recharge was based on a priori knowledge on the real dynamics of allogenic recharge that was derived from preceding experimental studies (Barberá et al., 2018; Mudarra et al., 2011). A smaller fraction $1/N$ still enters the fast and concentrated flow paths in the model. At karst systems, where entire rivers or large parts of their runoff water directly enter the karstic conduit system (i.e., Bailly-Comte et al., 2010, 2012; Dörfliger et al., 2008), a different model structure, which channels all allogenic recharge directly into the concentrated flow paths, would probably be more adequate.

As in previous studies (Hartmann et al., 2013; Hartmann, Mudarra, et al., 2014), tracer transport follows the assumptions of complete and instantaneous mixing for every model compartment, that is, the mass of tracer that enters one of the soil, epikarst, or groundwater storages of the $N$ model compartments mixes completely and instantaneously with the water (and stored tracer) within the storage. The path of the artificial tracer through the different model compartments, and the mixing within them, resembles the dispersion of the tracer. However, advection processes cannot be accounted for within the lumped structure of the model. We therefore only compare the observed and simulated shapes of the BTCs by aligning with a temporal shift (the observed mean transit time of the dye) applied to the simulated BTC.

#### 3.4.2. Parameter Estimation and Quantification of Uncertainty

Preceding studies showed that tracer data can be useful for the calibration and evaluation of hydrological models for karst systems (Oehlmann et al., 2015). Here information from the spring discharge data set and from the dye tracer experiment are jointly used to reduce the ambiguity in closing the simulated water balance. Nevertheless, the resolution of observed data, as well as the complex setting of the pilot site, creates a rather uncertain environment for modeling. For this reason, a new parameter estimation procedure was used to confine a large uniformly sampled set of model parameters, thus allowing some uncertainty to remain and also be quantified. To this end, KGE (Gupta et al., 2009) was chosen as measure of efficiency, defined by

$$\mathrm{KGE} = 1 - \sqrt{(r-1)^2 + (\alpha-1)^2 + (\beta-1)^2} \tag{3}$$

$$\text{with } \alpha = \frac{\sigma_S}{\sigma_O} \text{ and } \beta = \frac{\mu_S}{\mu_O} \tag{4}$$

Here $r$ is the linear correlation coefficient between simulations and observations, while $\mu_s/\mu_o$ and $\sigma_s/\sigma_o$ are the mean and standard deviation of simulations and observations, respectively. The $\alpha$ represents the variability; $\beta$ stands for the bias. By this definition, the best simulations are found with KGE close to 1. For the

**Table 2**
*Parameter Description, Units, Ranges, and Mean and Standard Deviation of the Remaining 35 Parameter Sets, Including Their Performance Concerning Spring Discharge ($KGE_Q$) and Tracer Simulations ($KGE_{BTC}$)*

| | | | Parameter ranges | | Estimated parameters and uncertainty | |
|---|---|---|---|---|---|---|
| Parameter | Description | Unit | Lower | Upper | Mean | Standard deviation |
| $A$ | Recharge area | $km^2$ | 5 | 15 | 7.4 | 1.5 |
| $Q_{river,max}$ | Maximum river infiltration | L/s | 0 | 15 | 0.9 | 0.5 |
| $V_{mean,S}$ | Mean soil storage capacity | mm | 0 | 1,000 | 442.1 | 274.7 |
| $V_{mean,E}$ | Mean epikarst storage capacity | mm | 0 | 1,000 | 785.7 | 185.2 |
| $a_{SE}$ | Soil/epikarst depth variability constant | — | 0 | 2 | 1.4 | 0.5 |
| $K_{mean,E}$ | Epikarst mean storage coefficient | day | 1 | 50 | 16.2 | 15.6 |
| $a_{fsep}$ | Recharge separation variability constant | — | 0 | 2 | 1.1 | 0.5 |
| $K_C$ | Conduit storage coefficient | day | 1 | 25 | 5.9 | 5.1 |
| $a_{GW}$ | Groundwater variability constant | — | 0 | 2 | 1.5 | 0.4 |
| $KGE_Q$ | Performance concerning discharge | — | 0 | 1 | 0.54 (0.59)[a] | 0.03 (0.21)[a] |
| $KGE_{BTC}$ | Performance concerning the tracer concentration | — | 0 | 1 | 0.60 | 0.06 |

*Note*. KGE = Kling-Gupta efficiency.
[a]Model performance during validation period (only available for discharge).

tracer BTC simulations, the highest value of cross correlation between simulated and observed tracer concentrations was preferable to *r*, since the model capability to include the spatial transport of the tracer from the injection point to the spring outlet is limited.

For calibration and quantification of uncertainty, an approach similar to that Hartmann et al. (2015) was used. An initial sample of 250,000 parameter sets was created applying a uniform Monte Carlo-based estimation sequence. They were tested uniformly from their predefined ranges (Table 2) in order to calculate KGE values concerning spring discharge ($KGE_Q$) and tracer BTC ($KGE_{BTC}$) for all. Then, existing field observations were gradually incorporated into the simulation procedure and the initial sample was reduced by iteratively applying three criteria (Figure 2):

1. The discharge criterion discards all parameter sets that obtain a $KGE_Q$ smaller than 0.5.
2. The tracer criterion discards all parameter sets that obtain a $KGE_{BTC}$ smaller than 0.5.
3. The combined criterion is the intersection of the discharge and the tracer criteria; that is, all simulations that simultaneously achieve $KGE_Q$ and $KGE_{BTC}$ larger or equal to 0.5.

As in previous works (Hartmann et al., 2013; Hartmann, Mudarra, et al., 2014), it can be expected that only hydrodynamic and tracer together data provide a realistic parameterization in the model. To show how discharge and dye information contribute to the simulation, this stepwise procedure is applied during which discharge or tracer data are first used for parameter estimation and, secondly, both simultaneously.

## 4. Results

### 4.1. Dye Tracer Test

After monitoring all the active outflow points in the Sierra de Enmedio and Los Tajos area, the dye injected to the Sabar streamflow was exclusively detected in the water drained by Auta spring, 120 hr after leakage and with the maximum concentration (0.46 μg/L) reached 183 hr after injection (Figure 3a). The fastest flow velocity deduced from these results was 26 m/hr, with a mean transit time of 17 m/hr. Uranine BTC (continuous recording) shows a well-defined main peak, followed by another smaller and poorly defined peak at 480–520 hr after injection (Figure 3a). Dye persisted in the spring water after the monitoring period, though at very low concentrations. The tracer test was carried out in a general hydrodynamic context of recession/beginning of depletion, as can be discerned by the decreasing trend of discharge values recorded at the outlet (Figure 3a). During this period mean flow rate, EC, and temperature values at the spring water were, respectively, 80 L/s, 599 μS/cm, and 17.0 °C.

No tracer was detected in the nearest spring to the injection point (Sabar outflow in Figure 3b) despite being at a lower altitude than Auta spring (Figure 1a). However, water samples containing uranine were taken in Sabar streamflow: in a section located 1 km downstream from the injection point (Figure 3b) where

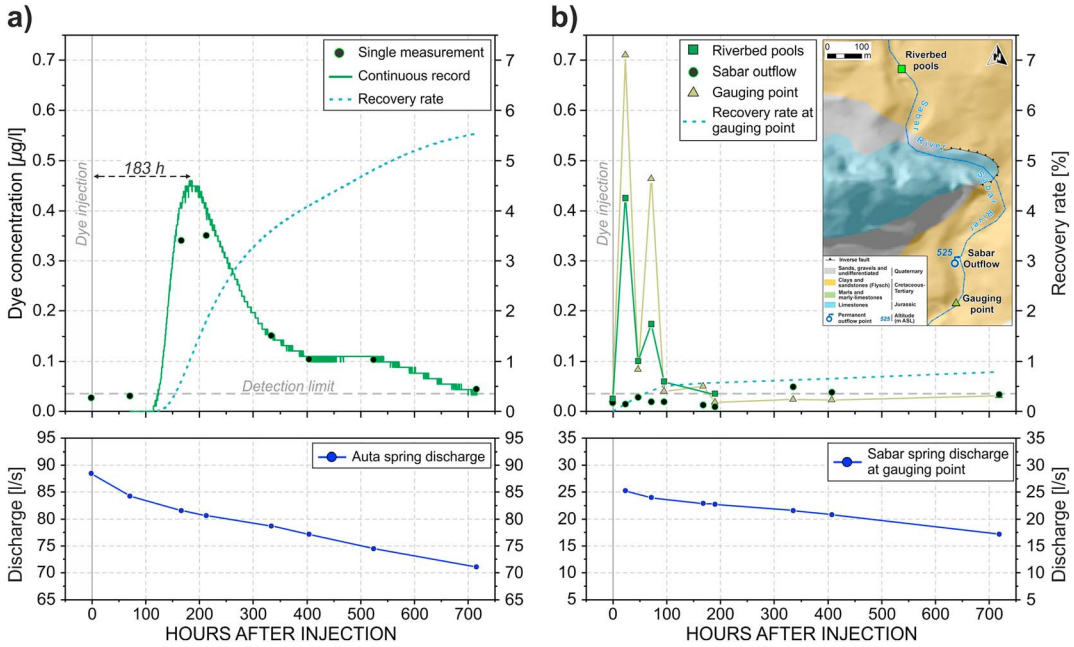


**Figure 3.** (a) Uranine breakthrough curve and recovery rate recorded and calculated, respectively, at the Auta spring in June 2011. (below) Discharge measured in the spring for the same period. (b) Uranine breakthrough curve recorded at the Sabar outflow water, at the stagnant riverbed pool, and at the gauging section in June 2011, jointly with the recovery rate calculated at the gauging section for the same period. (below) Discharge measured in the Sabar gauging section.

apparently stagnant water was found in pools (peak of 0.43 µg/L, 23 hr after injection) and also at a point placed 100-m downstream from Sabar spring (peak of 0.71 µg/L, 23 hr after injection) where outflow discharge was gauged (22 L/s of averaged rate). All this information indicates that a small portion of tracer mass (0.8% of recovery rate) did not infiltrate into the carbonates but was rapidly and subsuperficially transported downstream instead, flowing within the Quaternary alluvial materials. Averaged EC and temperature values recorded at the Sabar outflow water, at the stagnant riverbed pool and at the gauging section were, respectively, 1,468 µS/cm and 19.5 °C, 531 µS/cm and 20.2 °C, and 1430 µS/cm and 19.7 °C. Globally, the final recovery rate for uranine at the end of the test was 6.3% (32 g), which is very low.

### 4.2. Water Balance

#### 4.2.1. Discharge and Abstractions

During the study period, the natural discharge measured from all springs draining the Sierra de Enmedio and Los Tajos area amounted to 6.80 $hm^3$/year (Table 3), from which 2.82 $hm^3$/year corresponded to the average annual discharge of the Auta system. In addition, the mean rate of water extracted by pumping was around 0.65 $hm^3$/year; 0.15 $hm^3$/year derived from a borehole presumably drilled in the catchment area of the Auta spring, located 1,250-m upstream of the dye injection point (Figure 1a). Therefore, the mean total outflow identified from the Auta system was 2.97 $hm^3$/year (Table 3).

#### 4.2.2. Groundwater Autogenic Recharge

Mean annual values of diffuse aquifer recharge indirectly assessed after applying SWB and APLIS methods to the Sierra de Enmedio and Los Tajos area as a whole are summarized in Table 3. Under the first approach, 25 and 50 mm of UR values in the soil were considered, according to the edaphic properties of the experimental area. From these values, effective rainfall (equivalent to diffuse recharge) values between 412 and 363 mm/year were calculated, corresponding to 8.63 and 7.61 $hm^3$/year of total water resources, respectively. On the other hand, recharge rates between 20% and 80% of the rainfall were obtained with equation (1), equivalent to average value of 44.8%. The lowest recharge rates occur in Tertiary, Cretaceous-Tertiary, and Triassic outcrops of Figure 1a, while Quaternary deposits show moderate recharge rates. Medium to high recharge rates were detected in Jurassic carbonate outcrops, increasing at the northern edge of Los Tajos

**Table 3**
*Results From Water Budget Estimation in Sierra de Enmedio and Los Tajos Area, Where Auta System Is Included, During the Period 2006/2007–2008/2009*

| Discharge | | | | | |
|---|---|---|---|---|---|
| | | Hydrological year | | | Annual average ($hm^3$/year) |
| Regime | Spring name | 2006/2007 | 2007/2008 | 2008/2009 | |
| Natural | Batan | 1.75 | 1.44 | 2.74 | 1.98 |
| | Sabar | 0.98 | 0.54 | 1.43 | 0.98 |
| | Sierra del Rey | 0.17 | 0.15 | 0.68 | 0.33 |
| | **Auta** | **2.69** | **1.49** | **4.27** | **2.82** |
| | Others | 0.44 | 0.14 | 1.50 | 0.69 |
| Total | | 6.04 | 3.75 | 10.61 | 6.80 |
| Abstractions | **Auta system** | **0.15** | **0.15** | **0.15** | **0.15** |
| | Rest of the aquifer | 0.50 | 0.50 | 0.50 | 0.50 |
| Total | | 0.65 | 0.65 | 0.65 | 0.65 |
| Total outputs Sierra de Enmedio and Los Tajos area | | 6.69 | 4.40 | 11.26 | 7.45 |
| Auta system | | **2.84** | **1.64** | **4.42** | **2.97** |

| Recharge | | | | | | | | | | | |
|---|---|---|---|---|---|---|---|---|---|---|---|
| | Average precipitation (P) | | Soil Water Balance (SWB) | | | | | | APLIS method | | |
| | | | *UR* = 25 mm | | | *UR* = 50 mm | | | | | |
| Surface ($km^2$) | mm/year | $hm^3$/year | mm/year | $hm^3$/year | % *P* | mm/year | $hm^3$/year | % *P* | mm/year | $hm^3$/year | Recharge rate (% *P*) |
| 20.96 | 713 | 14.93 | 412 | 8.63 | 57.8 | 363 | 7.61 | 51.0 | 335 | 7.01 | 44.8 |

*Note*. Average rainfall calculated from isohyet maps. Diffuse recharge (expressed as mm/year and $hm^3$/year) calculated by Soil Water Balance and APLIS method. UR = useful reserve in the soil. Words and numbers in bold emphasis highlight the springs and the corresponding data that belong to hydrogeological system investigated in the article.

massif. Thus, water resources calculated by the APLIS method for the Sierra de Enmedio and Los Tajos area amount to 7.01 $hm^3$/year (Table 3).

The results obtained by the APLIS method are slightly lower than those estimated by the SWB approach with 50 mm of UR in the soil (7.61 $hm^3$/year), yet both are consistent with the total outputs (7.45 $hm^3$/year). However, since river infiltration from the Sabar head-basin partially contributes as allogenic nonquantified recharge to the Auta system, the values reached by APLIS method could be assumed, a priori, as the most suitable, being 0.44 $hm^3$/year (13.95 L/s) the average maximum contribution of river infiltration to the system recharge.

### 4.3. Numerical Modeling

The VarKarst model was used to reduce the uncertainty of the input components (runoff infiltration, recharge area, and recharge rates) in the water budget corresponding to the Auta system. The combined simulation of discharge and the artificial tracer, and the application of the three criteria specified at section 3.4.2, reduced the initial sample from 250,000 parameter sets to only 35 parameter sets (Figure 4). It is evident that the discharge criterion alone could still include substantial ambiguity (5,984 parameter sets). The tracer criterion alone (382 parameter sets) has a strong confining influence on the recharge rates and on maximum river infiltration, but it has no observable impact on assessment of the recharge area. Reasonable confinement for the recharge area, river infiltration, and recharge rate could only be attained using discharge and tracer information together for calibration. In this way, the originally wide ranges and uniformly distributed values of the input parameters are reduced to 7.4 ± 1.5 $km^2$ for the recharge area, 60.4 ± 7.9% (between 52.5–68.3%) for recharge rates, and 73.5 ± 41.6 $m^3$/day for maximum runoff infiltration. Although there is still some remaining uncertainty in the simulations of spring discharge and tracer BTC, the remaining 35 simulations envelop almost all of the observations of both variables (Figure 4).

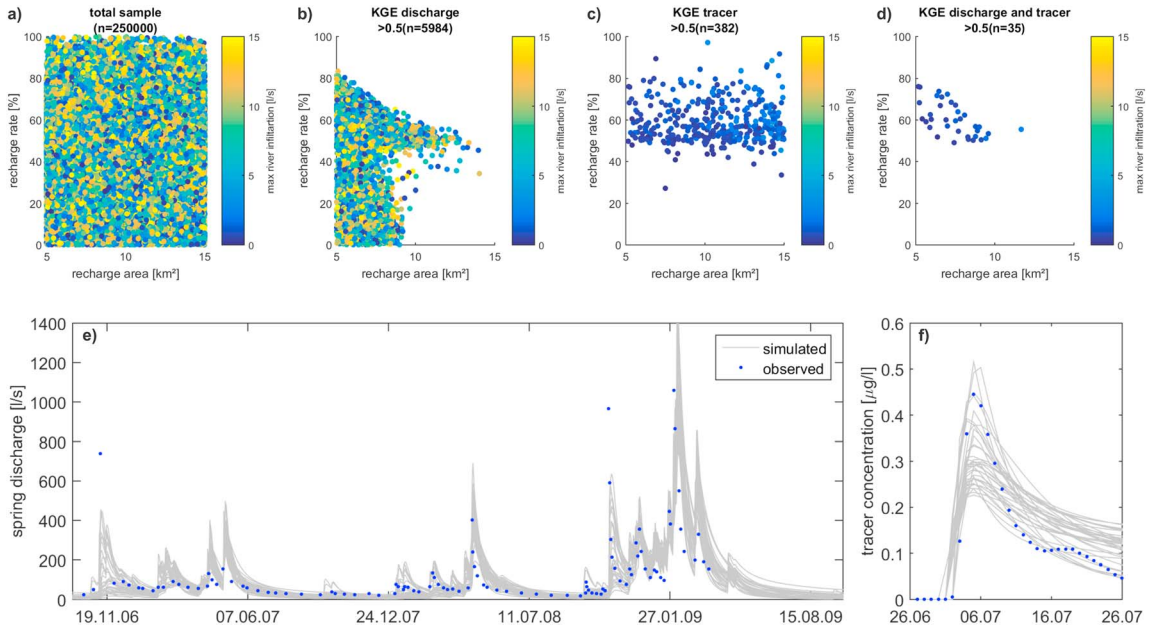


**Figure 4.** (top panels): Recharge areas, recharge rates, and maximum river infiltration $Q_{river,max}$ of the initial Monte Carlo sample (a), after applying discharge performance criterion (b), after applying the tracer performance criterion (c), and after applying the combined criteria (d); number $n$ in the title shows the size of the parameter set after the respective rule was applied. (bottom panels): (e) discharge and (f) tracer breakthrough curves simulated by the 35 remaining parameter sets after applying the combined criteria compared to observations. KGE = Kling-Gupta efficiency.

Considering uncertainty in this way, the VarKarst model provides a suitable and quantitative assessment of the input components of the pilot system. According to the modeling results, during the evaluation period 99.1% of total recharge occurred by diffuse means (2.99 ± 0.59 $hm^3$/year) and the remaining 0.9% represented the average recharge from water runoff (0.03 ± 0.02 $hm^3$/year).

## 5. Discussion

### 5.1. Water Budget Assessment and Numerical Modeling

Unlike many modeling approaches (Fleury et al., 2007; Long, 2015; Rimmer & Salingar, 2006), the main scope of the new version of the numerical code applied in this study was the assessment of the input components that take part in the water balance of a small karst system with unestablished catchment area but confirmed duality (autogenic and allogenic) in recharge mechanisms (binary karst system); features are commonly found in many karst aquifers worldwide. These components are partially represented by the model parameters (e.g., recharge area, maximum river infiltration, and partly by the recharge rate) derived from model internal fluxes. Since scarce field data are available, the Monte Carlo-based parameter estimation framework was believed to provide the most reliable results; by considering parameter uncertainty, it can quantify the information from instantaneous discharge measurements and from dye observations recorded during a specific hydrological condition, chosen for model calibration. Unlike the case of Liu et al. (2009), the procedure used did not result in an overall rejection of all parameter sets but rather a remainder of 35 parameter sets that produced acceptable simulations. Similar to Hartmann et al. (2015), the new parameter estimation procedure allowed the remaining prediction uncertainty to be quantified (Figure 4).

Evaluation with independent discharge data (hydrodynamic response of Auta system) indicates stability in obtained simulations, but there is also more variability in performance among the 35 simulations during the evaluation period (see standard deviation of KGE in Table 2). This indicates that the different hydroclimatic conditions affecting the system during this period provoke a decrease in model performance of at least some of the parameter sets, which is commonly found when a split sample test is applied (Klemeš, 1986; Perrin et al., 2003). Furthermore, because the numerical code simplifies groundwater flows though the unsaturated zone of the whole karst system, a reduction in the simulation capacities during the

recession limbs could be expected (Figure 4), due to the higher relative influence of this zone on the hydrodynamic behavior of the system under recession conditions (Mudarra et al., 2012). But as the mean of performance remains relatively stable, there are still enough signs that the parameter selection procedure provides reasonable and stable results. This is confirmed by the values of the model parameters (Table 2), whose ranges are similar to those obtained in other applications of the VarKarst model in the same region. While the soil and epikarst storage capacities ($V_{mean,S}$ and $V_{mean,E}$), as well as their variability constant ($a_{SE}$), are comparable to an application of the VarKarst model at the nearby and highly karstified Villanueva del Rosario system (Hartmann, Mudarra, et al., 2014), the groundwater variability constant ($a_{GW}$) and the epikarst storage coefficient ($K_{mean,E}$) more closely resemble an application of the numerical approach at another karst system in Southern Spain (Hartmann et al., 2013). The recharge separation variability constant ($a_{fsep}$) and the conduit storage coefficient ($K_C$) are enveloped by their corresponding values in both studies.

In detail, the ranges of calibrated values both for the recharge rate and for the recharge area are in accordance with field evidence and with the additional approaches used in this work, providing a consistent evaluation of the diffuse recharge (2.99 $\pm$ 0.59 $hm^3$/year) in the pilot site. A priori, either of the two independent methods—VarKarst and APLIS—were expected to give realistic rates, as both approaches were specifically designed for karst aquifers (Andreo et al., 2008; Hartmann et al., 2013). However, a more accurate range for the recharge rates was found using VarKarst code (52.5–68.3%) versus APLIS method (20–80%). Results from APLIS reflect the presence of areas with low recharge rates (associated with clays, sandstones, and marls in Figure 1a), outcropping into the limits established by the VarKarst model for the Auta system, and also beyond them, over the rest of the Sierra de Enmedio and Los Tajos area. In the case of the autogenic recharge area, its calibrated extent determined by the VarKarst model (7.4 $\pm$ 1.5 $km^2$) is slightly lower than the maximum apparent contributing area of carbonate outcrops to Auta spring (8.8 $km^2$). Unlike other karst systems where variations in simulated recharge area are often produced by changes in the hydroclimatic conditions during the calibration period (Hartmann et al., 2013; Jukic & Denić-Jukić, 2009), in the pilot site it is the strong influence of the geological structure in the hydrogeological behavior that restricts significant movements of groundwater divides. Rises in the piezometric level provoke only the gradual appearance of overflow springs in the discharge zone, from 620 m ASL to more than 640 m ASL.

With a calibrated mean value of 0.9 $\pm$ 0.5 L/s (0.03 $\pm$ 0.02 $hm^3$/year), the relative allogenic contribution of water runoff to the system recharge is clearly inferior to the average maximum value of the superficial allogenic input (13.95 L/s) that was indirectly inferred from the APLIS method and the water budget for the Sierra de Enmedio and Los Tajos area as a whole. The calibrated value is also slightly lower than infiltrated streamflow during tracer injection (3–4 L/s), although this rate is unrepresentative of the average annual conditions. In an additional attempt to confine further the remaining uncertainty in the quantification of the allogenic contribution to the spring discharge, modeling results were compared with calculations derived from the use of the coefficient of variations (CV%) of EC, following the equation defined by Worthington et al. (1992)

$$\%\text{Allog.contribution} = 3.57 \cdot \text{CV}\% - 13.57 \quad (5)$$

To perform this relationship, it was initially assumed that most of the variations in water mineralization of the spring were accounted for the proportion of autogenic versus allogenic infiltration sources. Single EC measurements recorded at the Auta and at the overflow springs during the study period were considered (Mudarra, 2012; Mudarra et al., 2012). According to equation (5), the water drained by the permanent outlet, with a 3.3% of CV (Figure 5), seems to have only an autogenic origin or a very limited influence of the allogenic component, whereas most of the overflow springs would be influenced in varying degrees (from 0.4%, OF4, to 29.6%, OF2, in Figure 5) by the concentrated infiltration coming from Sabar River, particularly under high flow conditions when they were active. Although these results appear as a good approximation to those inferred from the tracer test and from the VarKarst code, EC method loses reliability in the pilot site since interpretations about the variability of groundwater mineralization cannot be exclusively attributed to the contribution of different recharge mechanisms; other intrinsic factors that dominate the global system functioning must be invoked, which have significant impact on the hydrochemical response of the springs. In this way, it is well known that detailed monitoring and coupled analysis of the natural responses of the

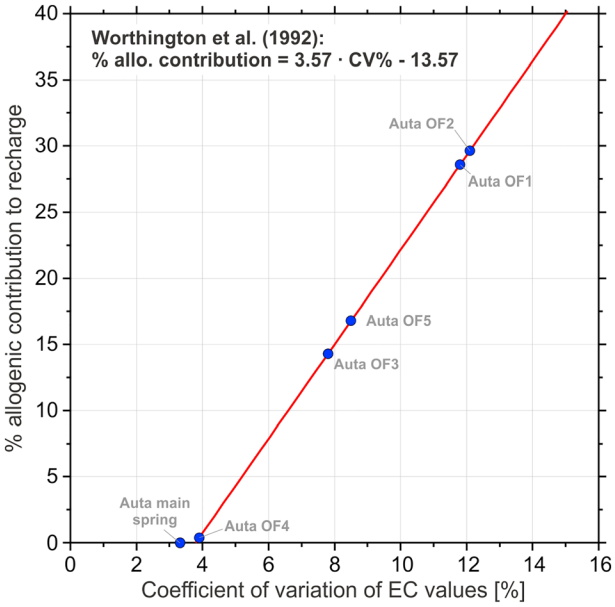


**Figure 5.** Estimations of the contribution of the allogenic and autogenic components to the total recharge of the Auta system, following the lineal relationship presented in Worthington et al. (1992): CV = 3.8 + 0.28% allogenic-contribution but adapted to EC series recorded in the water drained by the springs during the study period. EC = electrical conductivity; CV = coefficient of variations.

springs provide insights into the structure and dynamics of karst aquifers (Hunkeler & Mudry, 2007; Mudarra & Andreo, 2011), especially regarding the degree of development of the functional karstification within the unsaturated and the saturated zones and the modalities of infiltration (diffuse or concentrated). Likewise, the pilot site, there are many highly karstified carbonate aquifers worldwide (Mudarra et al., 2014; Perrin et al., 2007; Pinault et al., 2001) that show significant variations in discharge rate and in water mineralization whereas they are dominantly fed by upland autogenic and diffuse recharge types.

### 5.2. Modeling Considering River Infiltration and Dye Tracer

In general, after applying the combined criterion (discharge and dye tracer), the VarKarst model shows acceptable performance for discharge and uranine BTC simulations, despite the low recovery rate of uranine in Auta spring. The latter may be understood in the hydrodynamic context of depletion during which tracer experiment took place (Figure 3), with very low and slow flows in the Sabar River. Under this scenario, a fraction of fluorescent tracer dissolved in water runoff could be exposed to microbial activity and to the light photodegradation before being infiltrated along the carbonate outcrops in the riverbed (Benischke et al., 2007; Käss, 1998). In addition, a small portion of the tracer mass could be partially retained through the detrital sediments in the riverbed and then subsuperficially transported downstream as the sampling routine in Sabar River revealed (Figure 3b). The remaining quantity of uranine could be retained in conduits, fissures, and matrix within the unsaturated zone, affecting the transport dynamic and causing that only a small proportion of dye mass reached the groundwater level. Furthermore, the tailing effect observed in the Auta BTC (Figure 3a) suggests that the tracer movement within the saturated zone was certainly conditioned by dispersion mechanisms throughout the entire fracture network and also by the water transference between the mobile and immobile phases within the system (Massei et al., 2006). The rest of tracer mass could be drained by the spring in subsequent recharge events, although no information about this is available. Despite of the proximity to the sinking streambed, it is unlikely that fractions of uranine could be detected in other outflow points located at the Sierra de Enmedio and Los Tajos aquifer, due to the existence of hydraulic barriers (clays and marls) resulting of the geological complexity of the area. Otherwise, signals of pollution related to the waste water poured in the Sabar River head-basin would have been perceived in these springs (Mudarra, 2012).

The fact that the dye test results (flow velocity and recovery rate) are not illustrative of the wide range of hydrodynamic conditions (recharge, recession, and depletion) in the system reduces the model reliability in terms of the temporal variability with regard to the proportion of allogenic/autogenic recharges. Slightly higher values of concentrated infiltration should be expected particularly during recharge and recession periods attending (1) to the average results derived from the water balance for the aquifer as a whole and (2) to the better river-overflow spring connectivity due to the greater participation of the unsaturated flow in global system functioning under these conditions. The higher maximum values of contamination signs detected in the water drained by the overflow points (19.4 and 1.83 mg/L of $NO_3^-$ and TOC, respectively) versus by the permanent spring (14.4 and 1.12 mg/L) during the same periods tend to support previous assumption. Nevertheless, no markedly greater volume of water runoff infiltration should be invoked either, given the irregular hydrological regime of the river basin and the limited extension, moderate slope, and infiltration capacities of the carbonate outcrops in the riverbed (Figure 1).

Hence, calibrations of lumped models with field data from artificial tracer tests, such as in the current version of VarKarst model, provide more realistic results in the estimation of groundwater budget components than sole calibrations by discharge (Bishop et al., 2004; Kuczera & Mroczkowski, 1998; Son & Sivapalan, 2007), by hydrochemistry (Charlier et al., 2012; Hartmann et al., 2013; Hartmann, Mudarra, et al., 2014; Pinault et al., 2001), or by water isotopes (Maloszewski et al., 2002). The introduction of

specific variables and their combinations stands as a significant advance for simulation routines since each type of observations (natural and artificial) involves independent but complementary quantitative information for understanding the storage and infiltration dynamics of karst aquifers (Bakalowicz, 2005; Ford & Williams, 2007; White, 2002). This lends the model code greater capabilities in the representation of the recharge processes using relatively easy to obtain field data and, therefore, for assessing water resources in a wide range of hydrogeological scenarios and karst environments. Most lumped karst approaches consider concentrated infiltration without differentiating between internal and external runoff (e.g., Butscher & Huggenberger, 2008; Fleury et al., 2007). On the other hand, those who contemplate this division in the modeling performance of water balance (e.g., Jukic & Denić-Jukić, 2009) reached an acceptable estimation of the groundwater recharge components but only in aquifers clearly larger in size than the one exemplified here. Apart from lumped approaches, other methodologies broadly employed for evaluating the amounts of water derived from concentrated and diffuse recharge sources, such as the CV% of EC (White, 2002; Worthington et al., 1992) or conservative mixing equations (Binet et al., 2017; Doctor et al., 2006; Gill et al., 2018; Tobin & Schwartz, 2012), lead to rough estimations of the input components; water from different reservoirs usually does not have a uniform composition, and this can only be estimated approximately (Hunkeler & Mudry, 2007). All this reduces the reliability of the aforementioned methods, whose application should be restricted to a preliminary valuation of the recharge types. In contrast, our approach has demonstrated to hold the potential for inferring reliable quantitative information on the dynamics of recharge components (runoff infiltration, recharge area, and recharge rates) within the observed range of measurements.

In the current research, remaining uncertainty in the modeling routine might have been further reduced if hydrodynamic and hydrochemical data had been available in higher resolution (including the runoff component; e.g., see Kirchner & Neal, 2013) or if additional tracer tests could have been undertaken during different hydrological conditions. Ideally, ranges of calibrated values for recharge rate, recharge area, and, consequently, for maximum river infiltration could be constrained to reveal more information about water resources availability of the pilot system if isotopic data (from water runoff and the spring) were available in high temporal and spatial resolutions. Nevertheless, though observation availability and the hydrogeological heterogeneity introduce some biases into the model outputs, the equations and their combinations in the VarKarst code (Table 2 and Appendix A) reflect realities commonly found in any hydrological system. It would be expected, consequently, that more accurate estimations of the proportion of autogenic and allogenic recharge could be attained in karst aquifers characterized by a clear duality in recharge modalities using the approach presented here.

### 5.3. Coupling Conceptual and Numerical Models

Apart from its capacities on evaluation of water resources, results achieved by the VarKarst model can advance our knowledge of the hydrogeological functioning of karst aquifers, especially regarding the estimation of its effective autogenic recharge area. Integrating this quantitative information with previous (qualitative) findings from other experimental methodologies contributes to the development of a more realistic and robust conceptual model (Figure 6). Not only should the main vertically distributed features of the system (soil and epikarst, unsaturated zone, and phreatic zone) be considered but also the variability of infiltration and recharge modalities. For instance, the relative volume of specific autogenic recharge over the pilot site surface (inferred after applying the APLIS and the VarKarst methods) is now indicated in the new conceptualization (size and colors in arrows of Figure 6). Owing to the geological and hydrogeological complexities of the study site, it is unfortunately still not possible to represent faithfully the spatial distribution of the groundwater level and, therefore, of the groundwater flows by means of conceptual and numerical models. While significant progress in both directions has been made in the past few years (Hartmann, Goldscheider, et al., 2014), difficulties in collecting sufficient information about karst system properties persist, and the absence of reliable mathematical tools to predict their hydrogeological behavior hampers the simulation of spatially distributed aquifers, ultimately interfering with water management and planning initiatives.

The development of conceptual models prior to numerical modeling, with the intent of achieving a comprehensive understanding of groundwater flow behavior, is a necessary prerequisite for robust modeling (Beven, 2012). Knowledge of the geological and geomorphological framework, from which aquifer limits and geometry can be inferred, is essential (Goldscheider & Drew, 2007; Figures 2 and 6). Combining this information with temporal and spatial observation data series obtained from as many experimental

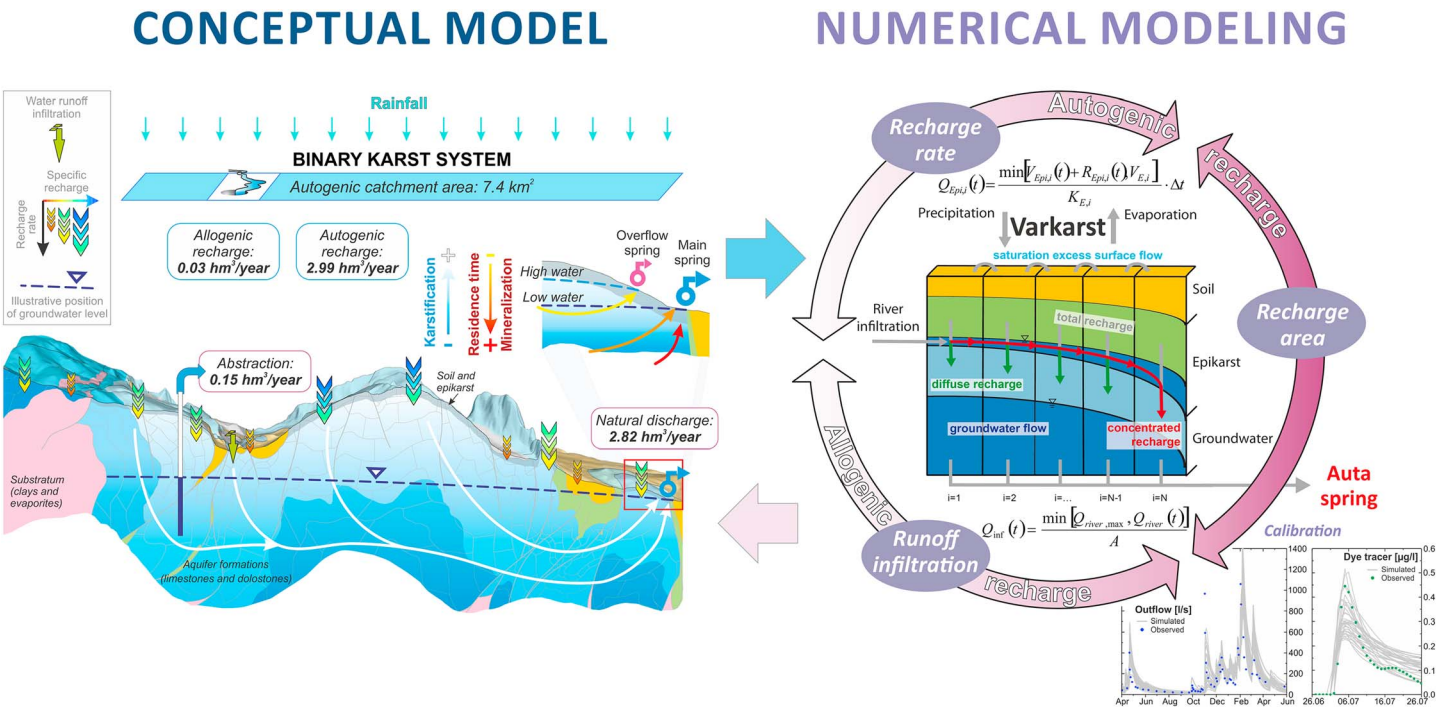


**Figure 6.** Schematic illustration of the integrated (conceptual and numerical) modeling approaches developed and applied in this study for the pilot karst system.

methods as possible (e.g., continuous monitoring of natural responses, isotopes, dye tests, hydraulic methods, and geophysical surveys) to jointly interpret results would allow researchers to schematize all distinctive elements that participate in the flow and storage patterns of the aquifers. From this information, numerical approaches can be developed and calibrated by means of the spatiotemporal resolution of relations expressed during the conceptualization, giving place to a quantitative solution of the hydrogeological processes that occur into the systems. The more information for researchers is available, the more reliable conceptualization will be possible, and therefore, a better numerical simulation of the hydrogeological behavior can be achieved. Nevertheless, transferring improvements from conceptual modeling to numerical approaches and vice versa (feedback) must be constantly conducted to enhance understanding of the hydrogeological systems and better manage water resources. During this process, it would be also necessary to check how feasible the adaptation from conceptual to numerical model (and vice versa) in different karst aquifers is, depending on their characteristics and functioning.

The results of the numerical simulation (and its intrinsic ambiguity) described in this paper may be very helpful to plan future research initiatives in the field, reinforcing the prediction capacities of new models (both conceptual and numerical). Such initiatives should include a continuous record of the hydrodynamic and hydrochemical responses of each overflow spring, which would enable a further comprehension of the duality of the preferential flow through conduits and diffuse flow through fissures and matrix within the aquifer. Likewise, hydrochemical and isotopic data from springs and particularly from the infiltration signal (experimental plots above the carbonate outcrops) would contribute to a more detailed spatiotemporal simulation/analysis of recharge and subsurface flow dynamics, also during varying hydroclimatic conditions. Finally, a better control of the streamflow of the Sabar River (continuous record) in the zone where infiltration has been confirmed would improve the estimation of the allogenic component using modeling tools such as VarKarst.

## 6. Conclusions

In this study, an improved version of the lumped-based VarKarst model was applied to jointly assess the contribution of different components (allogenic and autogenic) to the total recharge of a mountainous karst system with undefined catchment area and a certain complexity in its hydrogeological functioning. Spring discharge observations and results from a dye tracer experiment carried out in depletion conditions served

for model calibration and parameter estimation. Combining the two types of field information by means of a new parameter estimation procedure, the simulations confined the ambiguity detected in the general water balance performed with two other independent methods (SWB and APLIS). The obtained results show reliable ranges of calibrated values for the input parameters of the system, especially for recharge rate and recharge area, and to a lesser extent for maximum river infiltration. Likewise, the parameter confinement strategy enabled us to quantify the remaining uncertainty during recharge simulations.

These improvements upon the VarKarst model highlight that calibrating lumped-based models with data from artificial tracer tests can provide broader and more realistic results than calibrations solely by discharge or by hydrochemistry in the estimation of groundwater budget components. Furthermore, our approach is easily applicable for deducing reliable quantitative information on the recharge modalities in complex karst areas wherever other methodologies based on hydrochemical data lead to semiquantitative estimations of the input sources. Given the specific characteristics of dye tracers and their utility in karst hydrogeology, further specific procedures for the simulation and determination of hydraulic properties of carbonate aquifers can be expected using numerical models such as VarKarst.

The predictive value of an adequately calibrated numerical model makes it an excellent tool for planning the management of water resources under uncertain conditions. Models prove useful for assessing the vulnerability of karst aquifers to the expected consequences of climate change and to establish suitable adaptation strategies. However, numerical simulations will lose relevance for decision makers if there is a lack of integration and feedback in the realm of experimental methods, from which conceptual models and numerical approaches are derived. The use of different sources of information, characterizing techniques and modeling approaches (qualitatively and quantitatively), helps to reduce uncertainty in simulation routines, as demonstrated by the more detailed conceptual models presented here.

## Appendix A: Detailed Description of the VarKarst Model

The soil routine of the VarKarst model is controlled by the parameter $V_{\mathrm{mean,S}}$ (mm) and the distribution coefficient $a_{\mathrm{SE}}$ (−), which defines the variability of soil thicknesses across the $N = 15$ model compartments. The soil storage capacity $V_{\mathrm{S},i}$ (mm) for every compartment $i$ is then given by

$$V_{\mathrm{S},i} = V_{\mathrm{max,S}} \cdot \left(\frac{i}{N}\right)^{a_{\mathrm{SE}}} \tag{A1}$$

With $V_{\mathrm{max,S}}$ (mm) being the maximum soil storage capacity that is derived from $V_{\mathrm{mean,S}}$

$$\begin{gathered} \int_0^{i_{1/2}} V_{\mathrm{max,S}} \left(\frac{x}{N}\right)^{a_{\mathrm{SE}}} \mathrm{d}x = \frac{\int_0^{N} V_{\mathrm{max,S}} \left(\frac{x}{N}\right)^{a_{\mathrm{SE}}} \mathrm{d}x}{2} \;;\; V_{\mathrm{mean,S}} = V_{\mathrm{max,S}} \left(\frac{i_{1/2}}{N}\right)^{a_{\mathrm{SE}}} \\ \Updownarrow \\ V_{\mathrm{max,S}} = V_{\mathrm{mean,S}} \cdot 2^{\left(\frac{a_{\mathrm{SE}}}{a_{\mathrm{SE}}+1}\right)} \end{gathered} \tag{A2}$$

Here $i_{1/2}$ defines where the $V_{\mathrm{S},i}$ on the left equal the $V_{\mathrm{S},i}$ on the right (Figure 6). Parameter $a_{\mathrm{SE}}$ is also used to derive the epikarst maximum storage distribution by the mean epikarst depth $V_{\mathrm{mean,E}}$ (mm; derivation of $V_{\mathrm{max,E}}$ likewise to $V_{\mathrm{max,S}}$ in equation (2)

$$V_{\mathrm{E},i} = V_{\mathrm{max,E}} \cdot \left(\frac{i}{N}\right)^{a_{\mathrm{SE}}} \tag{A3}$$

At time $t$, actual evapotranspiration from each soil compartment $E_{\mathrm{act},i}$ is found by

$$E_{\mathrm{act},i}(t) = E_{\mathrm{pot}}(t) \cdot \frac{\min\left[V_{\mathrm{Soil},i}(t) + P(t) + Q_{\mathrm{Surface},i}(t),\ V_{\mathrm{S},i}\right]}{V_{\mathrm{S},i}} \tag{A4}$$

Thornthwaite's equation (Thornthwaite, 1948) is used to calculate daily potential evapotranspiration $E_{\mathrm{pot}}$ (mm). Surface runoff $Q_{\mathrm{surface},i}$ (mm) arrives from compartment *i-1* (see equation A9). We find recharge from the soil to the epikarst $R_{\mathrm{Epi},i}$ (mm) by

$$R_{\mathrm{Epi},i}(t) = Q_{\mathrm{inf}}(t) + \max\left[V_{\mathrm{Soil},i}(t) + P(t) + Q_{\mathrm{Surface},i}(t) - E_{\mathrm{act},i}(t) - V_{\mathrm{S},i},\ 0\right] \tag{A5}$$

$Q_{\mathrm{inf}}(t)$ is the river infiltration (mm/d; equation (2) in the main manuscript). Epikarst outflow dynamics are calculated using epikarst storage coefficients $K_{E,i}$ (day)

$$Q_{\mathrm{Epi},i}(t) = \frac{\min\left[V_{\mathrm{Epi},i}(t) + R_{\mathrm{Epi},i}(t), V_{\mathrm{E},i}\right]}{K_{\mathrm{E},i}}. \tag{A6}$$

$$K_{\mathrm{E},i} = K_{\mathrm{max,E}} \cdot \left(\frac{N - i + 1}{N}\right)^{a_{\mathrm{SE}}} \tag{A7}$$

$V_{\mathrm{Epi},i}$ (mm) represents the water volume within the epikarst at time step $t$. $K_{\mathrm{max,E}}$ is found by the mean epikarst storage coefficient $K_{\mathrm{mean,E}}$ and the distribution coefficient $a_{\mathrm{SE}}$

$$\begin{gathered} N \cdot K_{\mathrm{mean,E}} = \int_0^N K_{\mathrm{max,E}} \left(\frac{x}{N}\right)^{a_{\mathrm{SE}}} \mathrm{d}x \\ \Updownarrow \\ K_{\mathrm{max,E}} = K_{\mathrm{mean,E}} \cdot (a_{\mathrm{SE}} + 1) \end{gathered} \tag{A8}$$

Lateral surface runoff $Q_{\mathrm{Surf},i\ +\ 1}$ (mm) initiates when maximum soil and epikarst storage capacities are exceeded by the stored water volume

$$Q_{\mathrm{Surf},i+1}(t) = \max\left[V_{\mathrm{Epi},i}(t) + R_{\mathrm{Epi},i}(t) - V_{\mathrm{E},i},\ 0\right] \tag{A9}$$

Fast and diffuse recharge processes are accounted for by splitting vertical epikarst percolation into diffuse ($R_{\mathrm{diff},i}$ [mm]) and concentrated groundwater recharge ($R_{\mathrm{conc},i}$ [mm]) by a variable separation factor $f_{C,i}$ (−) and a distribution coefficient $a_f$ (−)

$$R_{\mathrm{conc},i}(t) = f_{C,i} \cdot Q_{\mathrm{Epi},i}(t) \tag{A10}$$

$$R_{\mathrm{diff},i}(t) = \left(1 - f_{C,i}\right) \cdot Q_{\mathrm{Epi},i}(t) \tag{A11}$$

$$f_{C,i} = \left(\frac{i}{N}\right)^{a_{f\mathrm{sep}}} \tag{A12}$$

The diffuse recharge component reaches the groundwater compartments $i = 1 \ldots N - 1$, while concentrated recharge laterally reaches to the conduit system (groundwater compartment $i = N$). Variable groundwater storage coefficients $K_{\mathrm{GW},i}$ (day) are found likewise to the soil and epikarst compartments. Matrix discharge is consequently found by

$$Q_{\mathrm{GW},i}(t) = \frac{V_{\mathrm{GW},i}(t) + R_{\mathrm{diff},i}(t)}{K_{\mathrm{GW},i}};\ \ i = 1 \ldots N-1 \tag{A13}$$

with

$$K_{\mathrm{GW},i} = K_C \cdot \left(\frac{i}{N}\right)^{-a_{\mathrm{GW}}} \tag{A14}$$

where conduit storage coefficient is given by $K_C$ (day). The conduit system from compartment $N$ accounts for the concentrated recharge component

$$Q_{\mathrm{GW},i}(t) = \frac{V_{\mathrm{GW},N}(t) + \sum_{i=1}^{N} R_{\mathrm{conc},i}(t)}{K_C};\ \ i = N \tag{A15}$$

The sum of all groundwater compartments finally gives the discharge of Auta spring $Q_{\mathrm{main}}$ (L/s) by rescaling it to (L/s) by the recharge area $A$ (km$^2$)

$$Q_{\text{main}}(t) = \frac{A_{\max}}{N} \cdot \sum_{i=1}^{N} Q_{\text{GW},i}(t) \quad \text{(A16)}$$

Tracer transport within the VarKarst model assumes complete mixing for every model compartment and is described in detail in the main body of the manuscript.

**Acknowledgments**
This work is a contribution to the projects CGL2012-32590 and CGL2015-65858R of the General Office of Scientific and Technical Research (DGICYT) of Spanish Government and to the Research Group RNM-308 funded by the Autonomous Government of Andalusia (Spain). We greatly thank Jens Lange for his kind and disinterested support in modeling performance tasks. The authors also thank anonymous reviewers for their constructive criticism which contributed to improving the original version of the manuscript. Improvements and suggestions done by Denis O'Carroll as Associated Editor are also much appreciated. Finally, we would like to acknowledge Jean Sanders for careful review of the English text. The field data used in this study were provided by the Department of Geology and Centre of Hydrogeology of the University of Malaga (CEHIUMA), Malaga 29071, Spain, and is available as supporting information.

## References

Andreo, B., Vías, J., Durán, J. J., Jiménez, P., López-Geta, J. A., & Carrasco, F. (2008). Methodology for groundwater recharge assessment in carbonate aquifers: Application to pilot sites in southern Spain. *Hydrogeology Journal*, *16*(5), 911–925. https://doi.org/10.1007/s10040-008-0274-5

Bailly-Comte, V., Borrell-Estupina, V., Jourde, H., & Pistre, S. (2012). A conceptual semidistributed model of the Coulazou River as a tool for assessing surface water–karst groundwater interactions during flood in Mediterranean ephemeral rivers. *Water Resources Research*, *48*, W09534. https://doi.org/10.1029/2010WR010072

Bailly-Comte, V., Martin, J. B., Jourde, H., Screaton, E. J., Pistre, S., & Langston, A. (2010). Water exchange and pressure transfer between conduits and matrix and their influence on hydrodynamics of two karst aquifers with sinking streams. *Journal of Hydrology*, *386*(1–4), 55–66. https://doi.org/10.1016/j.jhydrol.2010.03.005

Bakalowicz, M. (2005). Karst groundwater: A challenge for new resources. *Hydrogeology Journal*, *13*(1), 148–160. https://doi.org/10.1007/s10040-004-0402-9

Barberá, J. A., Mudarra, M., Andreo, B., & De la Torre, B. (2018). Diagnostic analysis of karst connections from tracing experiments: A dual analytical and modeling approach to solute transport characterization. *Hydrogeology Journal*, *26*(1), 23–40. https://doi.org/10.1007/s10040-017-1638-5

Benischke, R., Goldscheider, N., & Smart, C. (2007). Tracer techniques. In N. Goldscheider & D. Drew (Eds.), *Methods in karst hydrogeology* (pp. 147–170). London: Taylor & Francis.

Beven, K. (2012). *Rainfall-runoff modelling*. Chichester: John Wiley & Sons. https://doi.org/10.1002/9781119951001

Binet, S., Joigneaux, E., Pauwels, H., Albéric, P., Fléhoc, C., & Bruand, A. (2017). Water exchange, mixing and transient storage between a saturated karstic conduit and the surrounding aquifer: Groundwater flow modeling and inputs from stable water isotopes. *Journal of Hydrology*, *544*, 278–289. https://doi.org/10.1016/j.jhydrol.2016.11.042

Birk, S., Geyer, T., Liedl, R., & Sauter, M. (2005). Process-based interpretation of tracer tests in carbonate aquifers. *Groundwater*, *43*(3), 381–388.

Bishop, K., Seibert, J., Kohler, S., & Laudon, H. (2004). Resolving the double paradox of rapidly mobilized old water with highly variable responses in runoff chemistry. *Hydrological Processes*, *18*(1), 185–189. https://doi.org/10.1002/hyp.5209

Butscher, C., & Huggenberger, P. (2008). Intrinsic vulnerability assessment in karst areas: A numerical modeling approach. *Water Resources Research*, *44*, W03408. https://doi.org/10.1029/2007WR006277

Charlier, J. B., Bertrand, C., & Mudry, J. (2012). Conceptual hydrogeological model of flow and transport of dissolved organic carbon in a small Jura karst system. *Journal of Hydrology*, *460–461*, 52–64.

Doctor, D. H., Alexander, E. C. Jr., Petric, M., Kogovsek, J., Urbanc, J., Lojen, S., & Stichler, W. (2006). Quantification of karst aquifer discharge components through end-member mixing analysis using natural chemistry and isotopes as tracers. *Hydrogeology Journal*, *14*(7), 1171–1191. https://doi.org/10.1007/s10040-006-0031-6

Dörfliger, N., Fleury, P., & Ladouche, B. (2008). Inverse modeling approach to allogenic karst system characterization. *Groundwater*, *47*(3), 414–426. https://doi.org/10.1111/j.1745-6584.2008.00517.x

Drogue, C. (1980). Essai d'identification d'un type de structure de magasins carbonates fissurés. Application à l'interprétation de certains aspects du fonctionnement hydrogéologique. *Mémoires hors série Société Géologique de France*, *11*, 101–108.

Field, M. S., & Pinsky, P. F. (2000). A two-region nonequilibrium model for solute transport in solution conduits in karstic aquifers. *Journal of Contaminant Hydrology*, *44*(3–4), 329–351. https://doi.org/10.1016/S0169-7722(00)00099-1

Fleury, P., Ladouche, B., Conroux, Y., Jourde, H., & Dörfliger, N. (2009). Modelling the hydrologic functions of a karst aquifer under active water management. The Lez spring. *Journal of Hydrology*, *365*(3–4), 235–243. https://doi.org/10.1016/j.jhydrol.2008.11.037

Fleury, P., Plagnes, V., & Bakalowicz, M. (2007). Modelling of the functioning of karst aquifers with a reservoir model: Application to Fontaine de Vaucluse (South of France). *Journal of Hydrology*, *345*(1-2), 38–49. https://doi.org/10.1016/j.jhydrol.2007.07.014

Ford, D. C., & Williams, P. W. (2007). *Karst hydrogeology and geomorphology*. Chichester: John Wiley & Sons. https://doi.org/10.1002/9781118684986

Gerner, A., Schütze, N., & Schmitz, H. (2012). Portrayal of fuzzy recharge areas for water balance modelling. A case study in northern Oman. *Advances in Geosciences*, *31*, 1–7. https://doi.org/10.5194/adgeo-31-1-2012

Geyer, T., Birk, S., Licha, T., Liedl, R., & Sauter, M. (2007). Multi-tracer test approach to characterize reactive transport in karst aquifers. *Ground Water*, *45*(1), 36–45. https://doi.org/10.1111/j.1745-6584.2006.00261.x

Ghasemizadeh, R., Hellweger, F., Butscher, C., Padilla, I., Vesper, D., Field, M., & Alshawabkeh, A. (2012). Review: Groundwater flow and transport modeling of karst aquifers, with particular reference to the North Coast Limestone aquifer system of Puerto Rico. *Hydrogeology Journal*, *20*(8), 1441–1461. https://doi.org/10.1007/s10040-012-0897-4

Gill, L. W., Babechuk, M. G., Kamber, B. S., McCormack, T., & Murphy, C. (2018). Use of trace and rare earth elements to quantify autogenic and allogenic inputs within a lowland karst network. *Applied Geochemistry*, *90*, 101–114. https://doi.org/10.1016/j.apgeochem.2018.01.001

Goldscheider, N., & Drew, D. (Eds.) (2007). *Methods in karst hydrogeology*. Leiden: Taylor and Francis Group.

Goldscheider, N., Meiman, J., Pronk, M., & Smart, C. (2008). Tracer tests in karst hydrogeology and speleology. *International Journal of Speleology*, *37*(1), 27–40. https://doi.org/10.5038/1827-806X.37.1.3

Gupta, H. V., Kling, H., Yilmaz, K. K., & Martinez, G. F. (2009). Decomposition of the mean squared error and NSE performance criteria: Implications for improving hydrological modelling. *Journal of Hydrology*, *377*(1–2), 80–91. https://doi.org/10.1016/j.jhydrol.2009.08.003

Hartmann, A., Barberá, J. A., Lange, J., Andreo, B., & Weiler, M. (2013). Progress in the hydrologic simulation of time variant recharge areas of karst systems. Exemplified at a karst spring in southern Spain. *Advances in Water Resources*, *54*, 149–160. https://doi.org/10.1016/j.advwatres.2013.01.010

Hartmann, A., Gleeson, T., Rosolem, R., Pianosi, F., Wada, Y., & Wagener, T. (2015). A large-scale simulation model to assess karstic groundwater recharge over Europe and the Mediterranean. *Geoscientific Model Development*, *8*(6), 1729–1746. https://doi.org/10.5194/gmd-8-1729-2015

Hartmann, A., Goldscheider, N., Wagener, T., Lange, J., & Weiler, M. (2014). Karst water resources in a changing world: Review of hydrological modeling approaches. *Reviews of Geophysics*, *52*, 218–242. https://doi.org/10.1002/2013rg000443

Hartmann, A., Kobler, J., Kralik, M., Dirnböck, T., Humer, F., & Weiler, M. (2016). Model aided quantification of dissolved carbon and nitrogen release after windthrow disturbance in an Austrian karst system. *Biogeosciences*, *13*(1), 159–174. https://doi.org/10.5194/bg-13-159-2016

Hartmann, A., Lange, J., Weiler, M., Arbel, Y., & Greenbaum, N. (2012). A new approach to model the spatial and temporal variability of recharge to karst aquifers. *Hydrology and Earth System Sciences*, *16*(7), 2219–2231. https://doi.org/10.5194/hess-16-2219-2012

Hartmann, A., Mudarra, M., Andreo, B., Marín, A., Wagener, T., & Lange, J. (2014). Modeling spatiotemporal impacts of hydroclimatic extremes on groundwater recharge at a Mediterranean karst aquifer. *Water Resources Research*, *50*, 6507–6521. https://doi.org/10.1002/2014WR015685

Hunkeler, D., & Mudry, J. (2007). Hydrochemical methods. In N. Goldscheider & D. Drew (Eds.), *Methods in karst hydrogeology* (pp. 93–121). London: Taylor & Francis.

Jukic, D., & Denić-Jukić, V. (2009). Groundwater balance estimation in karst by using a conceptual rainfall-runoff model. *Journal of Hydrology*, *373*(3-4), 302–315. https://doi.org/10.1016/j.jhydrol.2009.04.035

Käss, W. (1998). *Tracing technique in geohydrology*. Rotterdam: Balkema.

Kiraly, L. (1998). Modelling karst aquifers by the combined discrete channel and continuum approach. *Bulletin d'Hydrogéologie*, *16*, 77–98.

Kirchner, J. W., & Neal, C. (2013). Universal fractal scaling in stream chemistry and its implications for solute transport and water quality trend detection. *Proceedings of the National Academy of Sciences of the United States of America*, *110*(30), 12,213–12,218. https://doi.org/10.1073/pnas.1304328110

Klemeš, V. (1986). Dilettantism in hydrology: Transition or destiny. *Water Resources Research*, *22*, 177S–188S. https://doi.org/10.1029/WR022i09Sp0177S

Kovacs, A., & Sauter, M. (2007). Modelling karst hydrodynamics. In N. Goldscheider & D. Drew (Eds.), *Methods in karst hydrogeology* (pp. 65–91). London: Taylor & Francis.

Kuczera, G., & Mroczkowski, M. (1998). Assessment of hydrologic parameter uncertainty and the worth of multiresponse data. *Water Resources Research*, *34*, 1481–1489. https://doi.org/10.1029/98WR00496

Le Moine, N., Andréassian, V., & Mathevet, T. (2008). Confronting surface- and groundwater balances on the La Rochefoucauld-Touvre karstic system (Charente, France). *Water Resources Research*, *44*, W03403. https://doi.org/10.1029/2007WR005984

Liu, Y., Freer, J., Beven, K., & Matgen, P. (2009). Towards a limits of acceptability approach to the calibration of hydrological models: Extending observation error. *Journal of Hydrology*, *367*(1–2), 93–103. https://doi.org/10.1016/j.jhydrol.2009.01.016

Long, A. J. (2015). RRAWFLOW: Rainfall-Response Aquifer and Watershed Flow Model (v1.15). *Geoscientific Model Development*, *8*(3), 865–880. https://doi.org/10.5194/gmd-8-865-2015

Luhmann, A. J., Covington, M. D., Alexander, S. C., Chai, S. Y., Schwartz, B. F., Groten, J. T., & Alexander, E. C. (2012). Comparing conservative and nonconservative tracers in karst and using them to estimate flow path geometry. *Journal of Hydrology*, *448–449*, 201–2211. https://doi.org/10.1016/j.jhydrol.2012.04.044

Maloszewski, P. (1994). Mathematical modelling of tracer experiments in fissured aquifers. *Freiburger Schriften zur Hydrologie*, 2, 1–107.

Maloszewski, P., Benischke, R., Harum, T., & Zojer, H. (1998). Estimation of solute transport parameters in a karstic aquifer using artificial tracer experiments. In P. Dillon & I. Simmers (Eds.), *Shallow Groundwater Systems, IAH International Contributions to Hydrogeology* (Vol. 18, pp. 177–190). London, UK: Taylor and Francis/Balkema.

Maloszewski, P., Stichler, W., Zuber, A., & Rank, D. (2002). Identifying the flow systems in a karstic-fissured-porous aquifer, the Schneealpe, Austria, by modelling of environmental $^{18}O$ and $^{3}H$ isotopes. *Journal of Hydrology*, *256*(1–2), 48–59. https://doi.org/10.1016/S0022-1694(01)00526-1

Mangin, A. (1975). Contribution à l'étude hydrodinamique des aquifères karstiques (I). *Annales Spéleologie*, *29*(3), 283–332; 29(4), 495–601; 30(1), 21–124.

Marín, A. I. (2009). The application of GIS to evaluation of resources and vulnerability to contamination of carbonated aquifer. Test site Alta Cadena (Malaga province), (MSc thesis). Malaga, Spain: University of Malaga.

Martín-Algarra, M. (1987). Evolución geológica alpina del contacto entre las Zonas Internas y Externas de la Cordillera Bética (PhD thesis). Granada, Spain: University of Granada.

Massei, N., Wang, H., Field, M., Dupont, J., Bakalowicz, M., & Rodet, J. (2006). Interpreting tracer breakthrough tailing in a conduit-dominated karst aquifer. *Hydrogeology Journal*, *14*(6), 849–858. https://doi.org/10.1007/s10040-005-0010-3

Mazzilli, N., Guinot, V., Jourde, H., Lecoq, N., Labat, D., Arfib, B., et al. (2017). KarstMod: A modelling platform for rainfall - discharge analysis and modelling dedicated to karst systems. *Environmental Modelling and Software*. https://doi.org/10.1016/j.envsoft.2017.03.015

Mazzilli, N., Jourde, H., Jacob, T., Guinot, V., Moigne, N., Boucher, M., et al. (2013). On the inclusion of ground-based gravity measurements to the calibration process of a global rainfall-discharge reservoir model: Case of the Durzon karst system (Larzac, southern France). *Environmental Earth Sciences*, *68*(6), 1631–1646. https://doi.org/10.1007/s12665-012-1856-z

Moore, R. J. (2007). The PDM rainfall-runoff model. *Hydrology and Earth System Sciences*, *11*(1), 483–499. https://doi.org/10.5194/hess-11-483-2007

Mudarra, M. (2012). Importancia relativa de la zona no saturada y zona saturada en el funcionamiento hidrogeológico de los acuíferos carbonáticos. Caso de la Alta Cadena, sierra de Enmedio y área de Los Tajos (provincia de Málaga), (PhD thesis). Malaga, Spain: University of Malaga.

Mudarra, M., & Andreo, B. (2011). Relative importance of the saturated and the unsaturated zones in the hydrogeological functioning of karst aquifers. The case of Alta Cadena (Southern Spain). *Journal of Hydrology*, *397*(3–4), 263–280. https://doi.org/10.1016/j.jhydrol.2010.12.005

Mudarra, M., Andreo, B., & Baker, A. (2011). Characterization of dissolved organic matter in karst spring waters using intrinsic fluorescence: Relationship with infiltration processes. *Science of the Total Environment*, *409*(18), 3448–3462. https://doi.org/10.1016/j.scitotenv.2011.05.026

Mudarra, M., Andreo, B., Marín, A. I., Vadillo, I., & Barberá, J. A. (2014). Combined use of natural and artificial tracers to determine the hydrogeological functioning of a karst aquifer: The Villanueva del Rosario system (Andalusia, southern Spain). *Hydrogeology Journal*, *22*(5), 1027–1039. https://doi.org/10.1007/s10040-014-1117-1

Mudarra, M., Andreo, B., & Mudry, J. (2012). Monitoring groundwater in the discharge area of a complex karst aquifer to assess the role of the saturated and unsaturated zones. *Environmental Earth Sciences*, *65*(8), 2321–2336. https://doi.org/10.1007/s12665-011-1032-x

Oehlmann, S., Geyer, T., Licha, T., & Birk, S. (2013). Influence of aquifer heterogeneity on karst hydraulics and catchment delineation employing distributive modeling approaches. *Hydrology and Earth System Sciences*, *17*(12), 4729–4742. https://doi.org/10.5194/hess-17-4729-2013

Oehlmann, S., Geyer, T., Licha, T., & Sauter, M. (2015). Reduction of the ambiguity of karst aquifer modeling through pattern matching of groundwater flow and transport. *Hydrology and Earth System Sciences*, *19*(2), 893–912. https://doi.org/10.5194/hess-19-893-2015

Padilla, A., & Delgado, J. (2013). TRASERO software. Treatment and management of temporal hydrological series (v2.0). Technical Report. Alicante, Spain: Diputación Provincial de Alicante.

Perrin, C., Michel, C., & Andréassian, V. (2003). Improvement of a parsimonious model for streamflow simulation. *Journal of Hydrology*, *279*(1-4), 275–289. https://doi.org/10.1016/S0022-1694(03)00225-7

Perrin, J., Jeannin, P. Y., & Cornaton, F. (2007). The role of tributary mixing in chemical variations at a karst spring, Milandre, Switzerland. *Journal of Hydrology*, *332*(1-2), 158–173. https://doi.org/10.1016/j.jhydrol.2006.06.027

Peyre, Y. (1974). Géologie d'Antequera et de sa région (Cordillères Bétiques, Espagne), (PhD thesis). Paris, France: University of Paris.

Pinault, J. L., Plagnes, V., Aquilina, L., & Bakalowicz, M. (2001). Inverse modeling of the hydrological and hydrochemical behaviour hydrosystems: Characterisation of karst system functioning. *Water Resources Research*, *37*, 2191–2204. https://doi.org/10.1029/2001WR900018

Rimmer, A., & Salingar, Y. (2006). Modelling precipitation-streamflow processes in karst basin: The case of the Jordan River sources, Israel. *Journal of Hydrology*, *331*(3-4), 524–542. https://doi.org/10.1016/j.jhydrol.2006.06.003

Rodríguez, L., Vives, L., & Gomez, A. (2013). Conceptual and numerical modeling approach of the Guarani Aquifer System. *Hydrology and Earth System Sciences*, *17*(1), 295–314. https://doi.org/10.5194/hess-17-295-2013

Saller, S. P., Ronayne, M. J., & Long, A. J. (2013). Comparison of a karst groundwater model with and without discrete conduit flow. *Hydrogeology Journal*, *21*(7), 1555–1566. https://doi.org/10.1007/s10040-013-1036-6

Scanlon, B. R., Mace, R. E., Barrett, M. E., & Smith, B. (2003). Can we simulate regional groundwater flow in a karst system using equivalent porous media models? Case study, Barton Springs Edwards aquifer, U.S.A. *Journal of Hydrology*, *276*(1–4), 137–158. https://doi.org/10.1016/S0022-1694(03)00064-7

Schmidt, S., Geyer, T., Guttman, J., Marei, A., Ries, F., & Sauter, M. (2014). Characterisation and modelling of conduit restricted karst aquifers. Example of the Auja spring, Jordan Valley. *Journal of Hydrology*, *511*, 750–763. https://doi.org/10.1016/j.jhydrol.2014.02.019

Schwerdtfeger, J., Hartmann, A., & Weiler, M. (2016). A tracer-based simulation approach to quantify seasonal dynamics of surface-groundwater interactions in the Pantanal wetland. *Hydrological Processes*, *30*(15), 2590–2602. https://doi.org/10.1002/hyp.10904

Seibert, J., & McDonnell, J. J. (2002). On the dialog between experimentalist and modeler in catchment hydrology: Use of soft data for multicriteria model calibration. *Water Resources Research*, *38*(11), 1241. https://doi.org/10.1029/2001WR000978

Son, K., & Sivapalan, M. (2007). Improving model structure and reducing parameter uncertainty in conceptual water balance models through the use of auxiliary data. *Water Resources Research*, *43*, W01415. https://doi.org/10.1029/2006WR005032

Thornthwaite, C. W. (1948). An approach toward a rational classification of climate. *Geographical Review*, *38*(1), 55–94. https://doi.org/10.2307/210739

Tobin, B., & Schwartz, B. (2012). Quantifying concentrated and diffuse recharge in two marble karst aquifers: Big Spring and Tufa Spring, Sequoia and Kings Canyon National Parks, California, USA. *Journal of Cave and Karst Studies*, *74*(2), 186–196. https://doi.org/10.4311/2011JCKS0210

Tritz, S., Guinot, V., & Jourde, H. (2011). Modelling the behavior of a karst system catchment using non-linear hysteretic conceptual model. *Journal of Hydrology*, *397*(3–4), 250–262. https://doi.org/10.1016/j.jhydrol.2010.12.001

White, W. B. (2002). Karst hydrology: Recent developments and open questions. *Engineering Geology*, *65*(2-3), 85–105. https://doi.org/10.1016/S0013-7952(01)00116-8

Worthington, S. R. H., Davies, G. J., & Quinlan, J. F. (1992). Geochemistry of springs in temperate carbonate aquifers: Recharge type explain most of the variation. In P. Chauve & F. Zwahlen (Eds.), *Proceeding of 5th conference on limestone hydrology and fissured media* (pp. 341–347). Neuchâtel, Switzerland: Universities of Neuchatel and Besançon.

Zagana, E., Tserolas, P., Floros, G., Katsanou, K., & Andreo, B. (2011). First outcomes from groundwater recharge estimation in evaporate aquifer in Greece with the use of APLIS method. In N. Lambrakis, G. Stournaras, & K. Katsanou (Eds.), *Advances in the research of aquatic environment* (pp. 89–96). Berlin, Germany: Springer. https://doi.org/10.1007/978-3-642-24076-8_11